

100-100000-100000  
R. B. 1573

Inactive

~~CONFIDENTIAL~~

Copy No. 50  
RM No. SL9A19

# NACA

## RESEARCH MEMORANDUM

for the

Bureau of Aeronautics, Department of the Navy  
LONGITUDINAL CHARACTERISTICS OF A SEMISPAN MODEL OF THE  
GRUMMAN AIRPLANE DESIGN 83 HAVING A SWEPTBACK WING AND  
OF THE MODEL WITH A STRAIGHT WING AS DETERMINED FROM  
WING-FLOW TESTS AT TRANSONIC SPEEDS

TED NO. NACA DE337

By

Norman S. Silsby and Robert M. Kennedy

Langley Aeronautical Laboratory  
Langley Air Force Base, Va.

CLASSIFIED DOCUMENT

This document contains classified information affecting the National Defense of the United States within the meaning of the Espionage Act, USC 793 and 794. Its transmission or the revelation of its contents in any manner to an unauthorized person is prohibited by law. Information so classified may be imparted only to persons in the military and naval services of the United States, appropriate civilian officers and employees of the Federal Government who have a legitimate interest therein, and to United States citizens of known loyalty and discretion who of necessity must be informed thereof.

NATIONAL ADVISORY COMMITTEE  
FOR AERONAUTICS  
WASHINGTON

CLASSIFICATION CANCELLED

Authority *2000-127-2199* Date *1/11/53*

By *2000-127-2199* See *1/24/55*

UNCLASSIFIED



UNCLASSIFIED

NATIONAL ADVISORY COMMITTEE FOR AERONAUTICS

RESEARCH MEMORANDUM

for the

Bureau of Aeronautics, Department of the Navy

LONGITUDINAL CHARACTERISTICS OF A SEMISPAN MODEL OF THE  
GRUMMAN AIRPLANE DESIGN 83 HAVING A SWEEPBACK WING AND  
OF THE MODEL WITH A STRAIGHT WING AS DETERMINED FROM  
WING-FLOW TESTS AT TRANSONIC SPEEDS

TED NO. NACA DE337

By Norman S. Silsby and Robert M. Kennedy

SUMMARY

An investigation has been made by the NACA wing-flow method to provide information on the relative longitudinal characteristics of a straight and sweptback wing in the transonic speed range. Tests were made of a semispan model of the Grumman airplane design 83 (XF10F) incorporating a wing swept back  $42.5^\circ$  with reference to quarter-chord line and also of the model with the swept wing replaced by a straight wing similar to that of the XF9F airplane. The airfoil sections were symmetrical  $64_1$ -series, with thickness ratios of 12 percent for the straight wing and 10 percent for the sweptback wing parallel to the stream direction. Measurements were made of normal force, chord force, and pitching moment at various angles of attack with the two wings both with and without the empennage, and with the fuselage alone. The tests covered a range of effective Mach numbers at the wing of the model from 0.65 to 1.10.

INTRODUCTION

At the request of the Bureau of Aeronautics, wing-flow tests have been made in the transonic speed range to compare the longitudinal characteristics of a model of the Grumman airplane design 83 (XF10F) equipped with both a straight and a wing sweptback  $42.5^\circ$  with reference to quarter-chord line.

UNCLASSIFIED

Measurements were made of normal force, chord force, and pitching moment at various angles of attack with the two wings both with and without the empennage, and with the fuselage alone. The tests covered a range of effective Mach numbers at the wing of the model from 0.65 to 1.10.

In the interest of expediting this paper, the data are presented without analysis.

### SYMBOLS

$\alpha$	angle of attack of fuselage, degrees
$\Delta\alpha$	difference in flow direction between wing and tail of model, degrees
$M_L$	local Mach number at wing surface of F-51D airplane
$M_w$	effective Mach number at wing of model
$M_t$	effective Mach number at tail of model
$V$	velocity, feet per second
$q$	effective dynamic pressure, pounds per square foot $\left(\frac{1}{2}\rho V^2\right)$
$S$	wing area, semispan, square feet
$\bar{c}$	mean aerodynamic chord of wing; based on the relationship $\int_0^b \frac{c^2 dy}{S}$ where $b$ is wing span and $c$ is chord, inches
$N$	normal force, pounds
$D$	drag force, pounds (resultant force parallel to stream velocity)
$M$	pitching moment, inch-pounds
$C_N$	normal-force coefficient $(N/qS)$
$C_D$	drag coefficient $(D/qS)$

$C_{m0.40\bar{c}}$	pitching-moment coefficient referred to 0.40 $\bar{c}$ ( $M/qS\bar{c}$ )
$R_w$	Reynolds number of wing based on mean aerodynamic chord $\bar{c}$
$R_t$	Reynolds number of tail based on mean aerodynamic chord of tail
$\frac{\partial C_N}{\partial \alpha}$	slope of normal-force curve per degree for $C_N = 0$
$\left(\frac{\partial C_m}{\partial C_N}\right)_{0.40\bar{c}}$	slope of pitching-moment curve referred to 0.40 $\bar{c}$ at $C_N = 0$

## APPARATUS AND TESTS

The tests were made, as described in references 1 and 2, by the NACA wing-flow method in which the model is mounted in the high-speed flow over the wing of an F-51D airplane.

Photographs of the semispan model equipped with an end plate at the fuselage center line are given in figures 1 and 2. The geometric characteristics of the model and each wing tested are given in table I; other details of the model and wings are shown in figure 3. The airfoil sections are 64<sub>1</sub>-series with thickness ratios of 12 percent for the straight wing and 10 percent for the sweptback wing parallel to the stream direction. The aspect ratios of the wings, considering the airplane wing surface as a reflection plane, are 2.5 for the sweptback wing and 4.97 for the straight wing. The model was mounted close to the airplane wing, and the shank of the model, which passed through a slot in the wing, was mounted on a strain-gage balance. Because the model and balance were arranged to oscillate as a unit, the balance measured the forces both normal and parallel to the fuselage reference line of the model at all angles of attack. The configurations tested were the semispan design 83 model with the sweptback wing and with the straight XF9F wing both with and without the empennage, and the semispan fuselage alone. For each test, continuous measurements were made of angle of attack, normal force, chord force, and pitching moment as the model was oscillated through a range of angles of attack of the fuselage reference line from about  $-7.5^\circ$  to  $4.5^\circ$ . Since the incidence of both wings was  $4.5^\circ$ , the range of angles of attack of the wings was from about  $-3^\circ$  to  $9^\circ$ . A free floating vane was used to determine the correct angle of attack of the model as described in reference 3.

The chordwise velocity gradients in the test region on the airplane wing as determined from static pressure measurements at the wing surface with the model removed are indicated in figure 4. The effective dynamic pressure  $q$ , the effective Mach number at the model wing  $M_w$ , and the effective Mach number at the model tail  $M_t$  were determined from an integration of the velocity distribution over the area covered by the wing and tail of the model. The variation of Mach number at the tail  $M_t$  with Mach number at each wing  $M_w$ , due to the chordwise velocity gradient, is shown in figure 5. A more complete discussion of the method of determining the Mach number and dynamic pressure at the model can be found in reference 3.

The tests were made by diving the F-51D airplane from an altitude of about 24,000 feet to about 15,000 feet, at which altitude an airplane Mach number of 0.73 was attained and the records started. The dive was then continued at an indicated speed of about 450 miles per hour and a pull-out to level flight effected at an altitude of about 5000 feet. In the level-flight portion of the test the airplane was allowed to decelerate to a Mach number of 0.5, at which Mach number the records were discontinued. This test procedure permits the maximum Reynolds number to be obtained at a given Mach number within the placard limits of the airplane. The average relation between Reynolds number at the wings  $R_w$  and the Reynolds number at the tail  $R_t$  with the Mach number at the wing  $M_w$  is shown in figure 6.

During the course of the investigation it was found that a curvature in the flow direction existed at the model station on the wing, resulting in a difference in flow angle between the wing and tail locations of the model (about 45 and 51 percent, respectively, of the airplane wing chord at the test station). The variation of this difference in flow angle with Mach number is shown in figure 7. This difference in flow angle between the wing and tail would effectively change the longitudinal characteristics of the model the same as increasing the incidence of the stabilizer by a similar amount.

#### PRESENTATION OF RESULTS

The variation of normal-force coefficient with angle of attack at several Mach numbers for the complete model with the swept and the straight wing is shown in figure 8. The variation of normal-force coefficient with angle of attack at various Mach numbers for the model with each of the two wings but without the empennage is shown in figure 9. In figures 8 and 9 and in subsequent figures where basic data are presented, the data are for

one complete cycle of increasing and then decreasing angle of attack during which the Mach numbers decreased slowly. The Mach number indicated in these figures is an average Mach number for the given cycle and is within  $\pm 0.005$  of the Mach number for any portion of the cycle.

A cross plot of figures 8 and 9 is presented in figure 10 to show the variation with Mach number of angle of attack at various normal-force coefficients for the model with and without empennage.

The variation with Mach number of the rate of change of normal-force coefficient with angle of attack  $\frac{\partial C_N}{\partial \alpha}$  is presented in figure 11 for the complete model with each wing both with and without the empennage.

The variation of pitching-moment coefficient with normal-force coefficient at several Mach numbers for the complete model with each wing is shown in figure 12. The variation of pitching-moment coefficient with normal-force coefficient at several Mach numbers for the model with each wing but without the empennage is presented in figure 13.

A cross plot of figures 12 and 13 is presented in figure 14 to show the variation with Mach number of the pitching-moment coefficient at several normal-force coefficients.

The variation of pitching-moment coefficient with angle of attack at various Mach numbers is presented in figure 15 for the complete models, in figure 16 for the models without the empennage, and in figure 17 for the semispan fuselage alone.

The variation with Mach number of the rate of change of the pitching-moment coefficient with normal-force coefficient  $\left( \frac{\partial C_m}{\partial C_N} \right)_{0.40\bar{C}}$  at  $C_N = 0$  for the complete models is shown in figure 18.

The variation of drag coefficient with Mach number for several normal-force coefficients is given in figure 19 for the various configurations tested.

A comparison of the drag coefficients of the model with and without empennage and of the fuselage alone is presented in figure 20. The drag coefficient of the fuselage alone in figure 20(a) is based on the area of the swept design 83 wing and that in figure 20(b) on the area of the straight XF9F wing. The area of each wing includes the area of the fuselage between the extensions of the leading and trailing edges to the plane of symmetry.

The drag of the fuselage alone (fig. 20) appears to be high. In other wing-flow tests on the drag of a body of revolution, the drag was higher than that of a similar body obtained by free-fall tests (unpublished data). However, the general shape of the drag curve and the over-all drag rise obtained on the wing-flow body compared well with those of the free-fall tests. It is therefore believed that while the fuselage drag in the present tests is high, the variation of drag with Mach number and the total drag rise are of the correct order of magnitude.

Langley Aeronautical Laboratory  
National Advisory Committee for Aeronautics  
Langley Field, Va.

*Norman S. Silsby*

Norman S. Silsby  
Aeronautical Research Scientist

*Robert M. Kennedy*

Robert M. Kennedy  
Aeronautical Engineer

Approved:

*Melvin N. Gough*

Melvin N. Gough  
Chief of Flight Research Division

JSF

REFERENCES

1. Zalovcik, John A., and Sawyer, Richard H.: Longitudinal Stability and Control Characteristics of a Semispan Airplane Model at Transonic Speeds from Tests by the NACA Wing-Flow Method. NACA ACR No. L6E15, 1946.
2. Zalovcik, John A., and Sawyer, Richard H.: Longitudinal Stability and Control Characteristics of a Semispan Airplane Model with a Swept-Back Tail from Tests at Transonic Speeds by the NACA Wing-Flow Method. NACA RM No. L6K21, 1946.
3. Johnson, Harold I.: Measurements of Aerodynamic Characteristics of a 35° Sweptback NACA 65-009 Airfoil Model with  $\frac{1}{4}$ -Chord Plain Flap by the NACA Wing-Flow Method. NACA RM No. L7F13, 1947.

TABLE I

GEOMETRIC CHARACTERISTICS OF  $\frac{1}{50}$ -SCALE SEMISPAN MODEL OF GRUMMAN

## AIRPLANE DESIGN 83 AND STRAIGHT WING SIMILAR TO XF9F

Wing dimension	Straight wing    Design 83 wing	
	64 <sub>1</sub> -A012	64 <sub>1</sub> -A010
Section . . . . .		
Semispan, in. . . . .	4.23	3.55
Mean aerodynamic chord, in. . . . .	1.80	2.93
Chord at tip, in. . . . .	1.06	2.08
Chord at plane of symmetry, in. . . . .	2.37	3.64
Area (semispan), sq in. . . . .	7.2	10.1
Aspect ratio . . . . .	4.97	2.5
Taper ratio . . . . .	0.46	0.572
Sweepback (0.25 chord line), deg . . . .	0	42.5
Dihedral (chordal plane), deg . . . . .	4	0
Incidence (chordal plane), deg . . . . .	4.5	4.5
Horizontal tail (geometrically similar to design 83 wing)		
Section . . . . .	62-A010	
Semispan, in. . . . .	1.67	
Mean aerodynamic chord, in. . . . .	1.38	
Chord at tip, in. . . . .	0.978	
Chord at plane of symmetry, in. . . . .	1.71	
Area (semispan), sq in. . . . .	2.22	
Aspect ratio . . . . .	2.5	
Incidence (chordal plane), deg . . . . .	4.5	
Length (0.25 wing to 0.25 tail), in. . . .	5.08	
Height (above wing chord), in. . . . .	2.11	



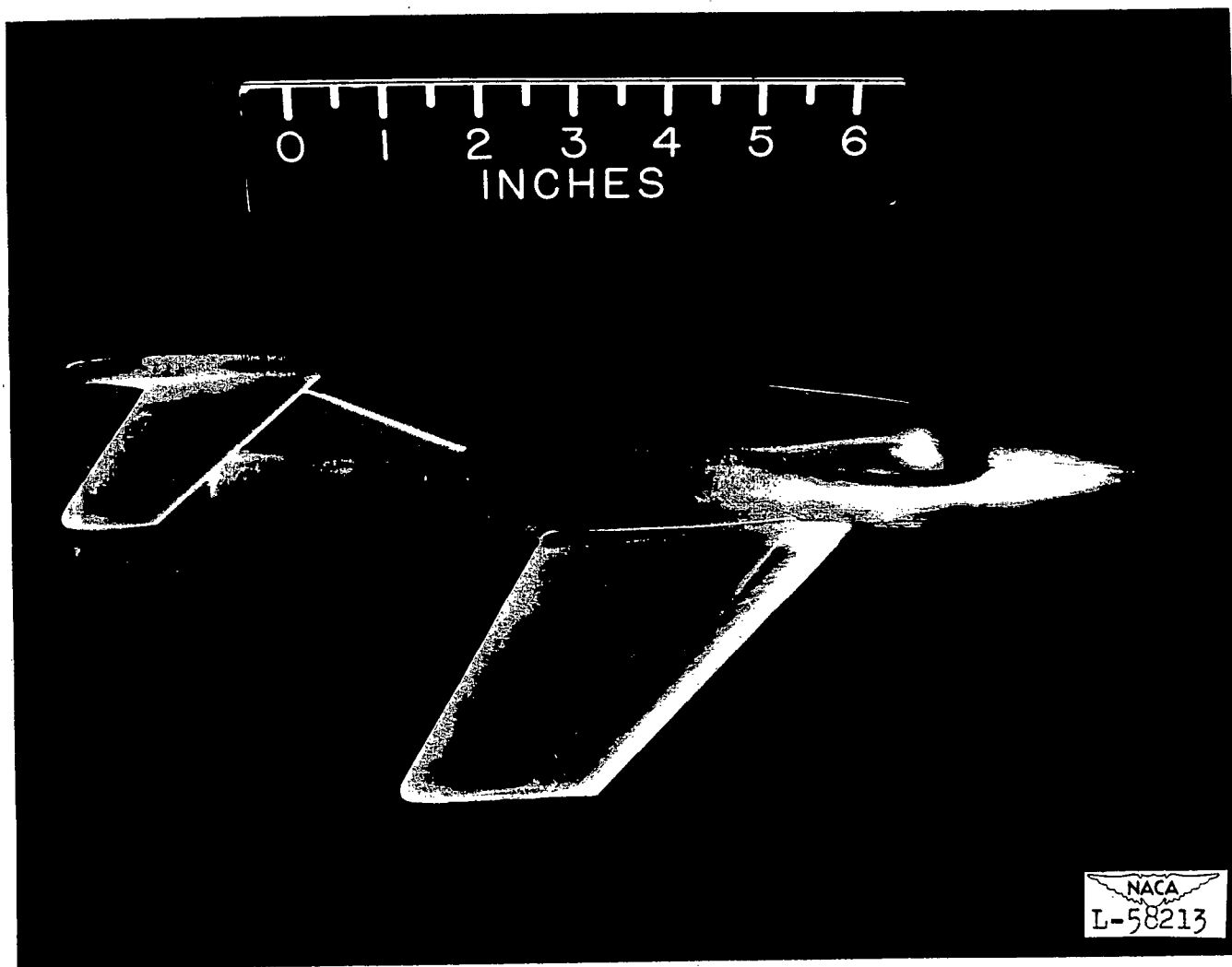


Figure 1.- Semispan model of the Grumman airplane design 83 equipped with a sweptback wing.

~~CONFIDENTIAL~~

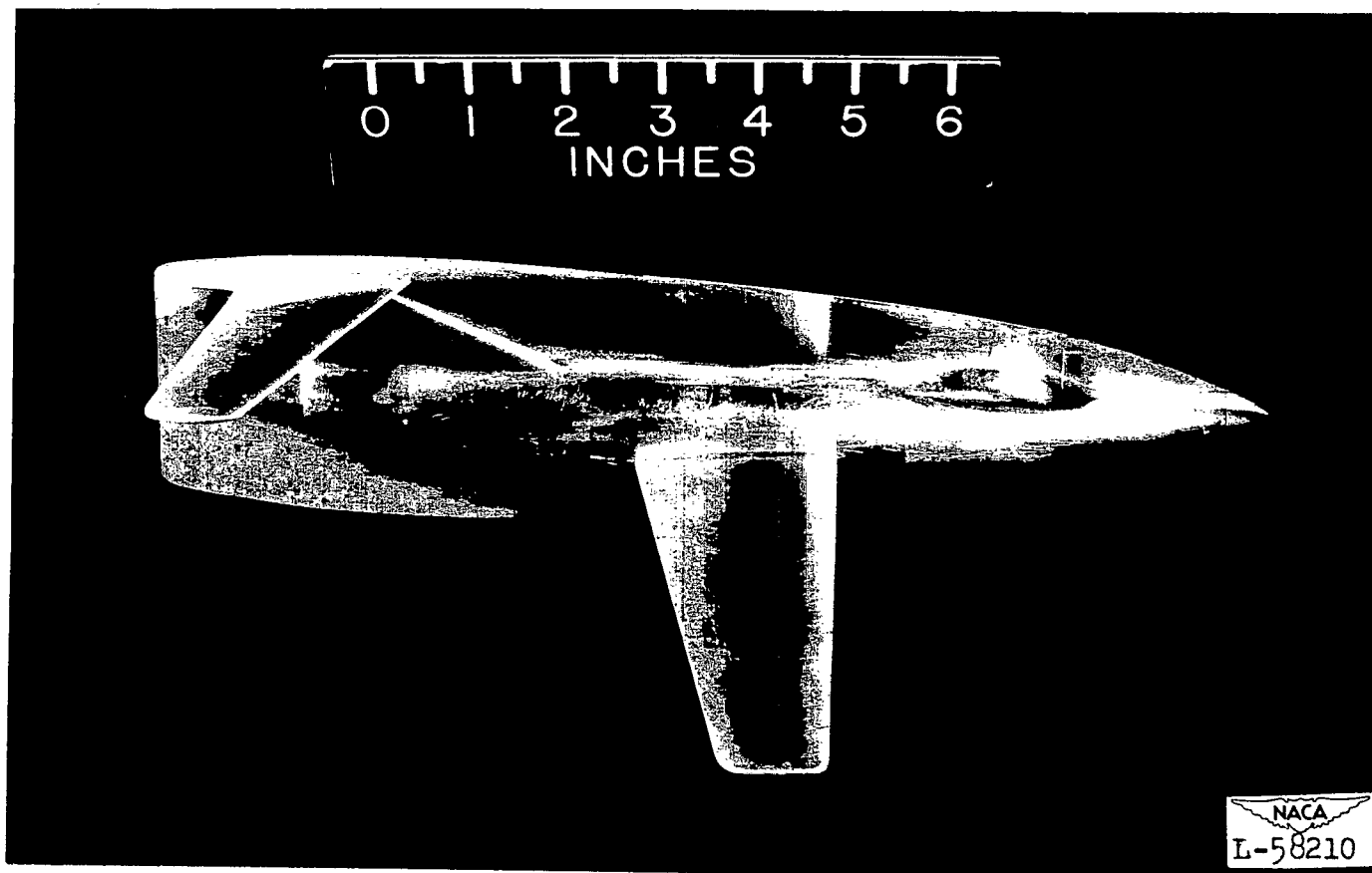
~~CONFIDENTIAL~~

Figure 2.— Semispan model of the Grumman airplane design 83 equipped with an unswept wing.

~~CONFIDENTIAL~~

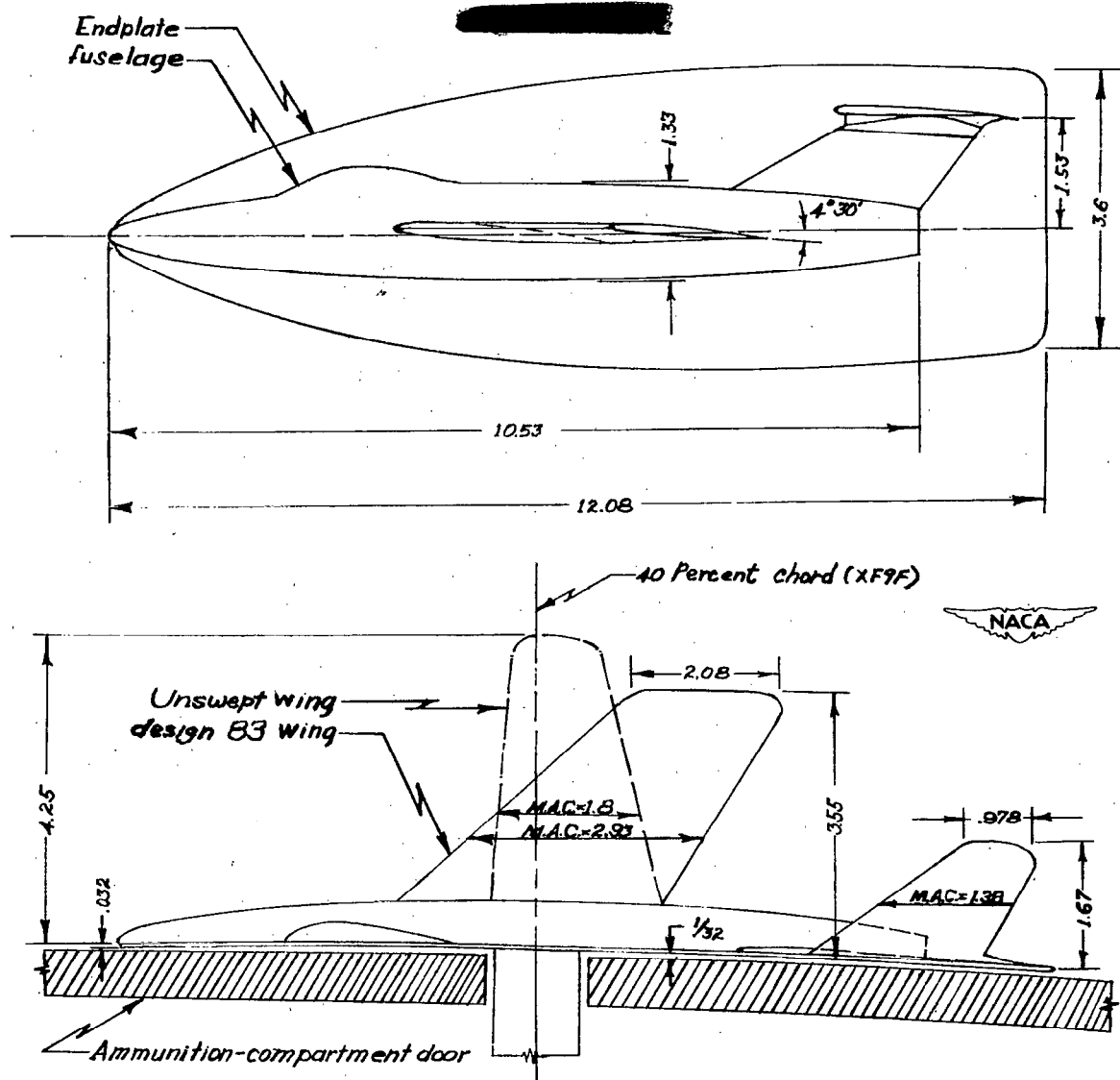


Figure 3.— Details of semispan model of Grumman airplane design 83 with unswept wing shown dotted. (All dimensions are in inches.)

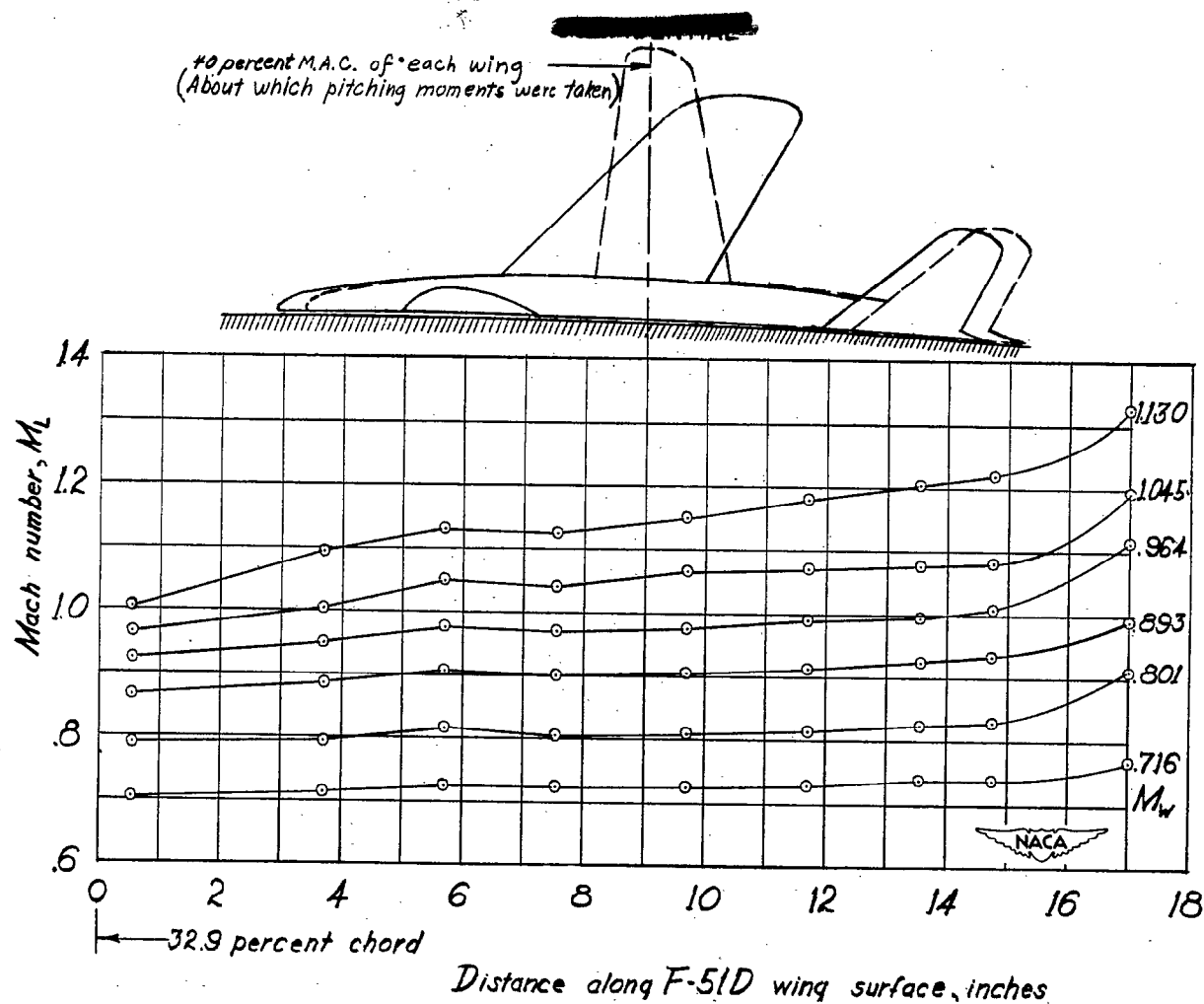


Figure 4.— Typical chordwise variation of local Mach number in the test region on the surface of airplane wing for several Mach numbers  $M_w$  at the unswept model wing. Chordwise location of model with each wing also shown.

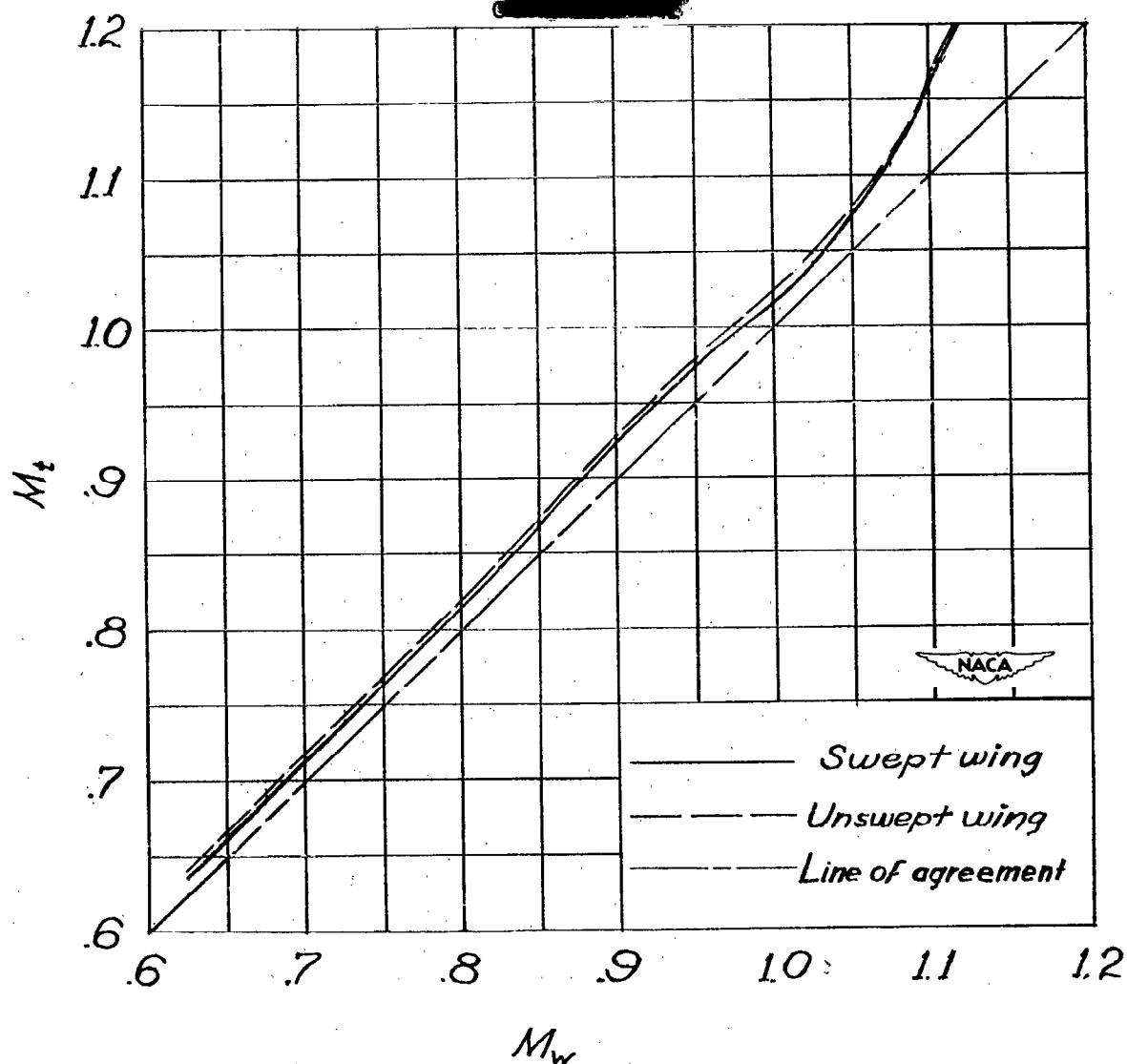


Figure 5.— Variation of Mach number at the tail  $M_t$  with Mach number at the wing  $M_w$  for both the swept and the unswept wings. Line of agreement also shown.

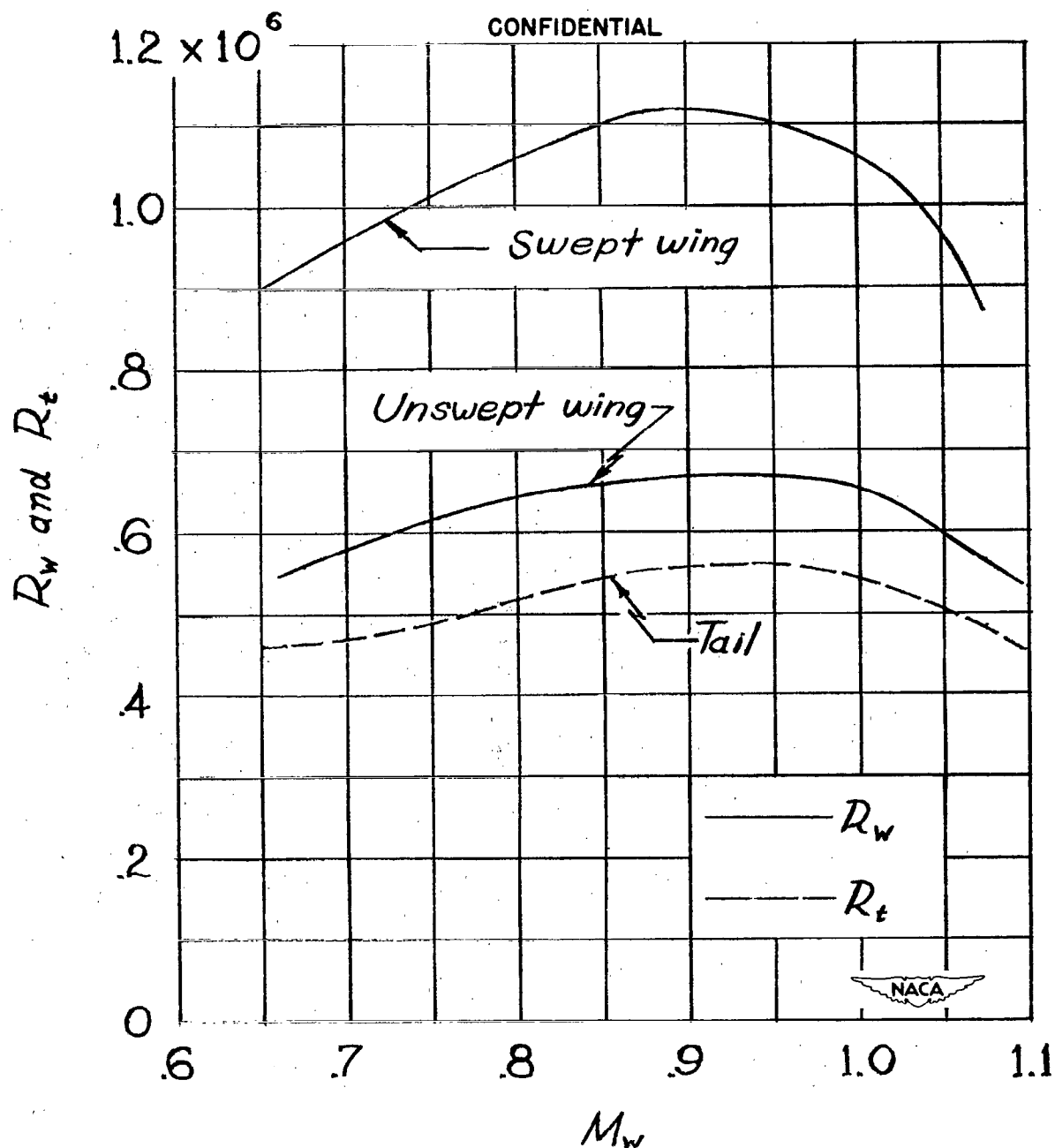


Figure 6.— Variation of Reynolds number of wing  $R_w$  and Reynolds number of tail  $R_t$  with Mach number at the wing  $M_w$ .

CONFIDENTIAL

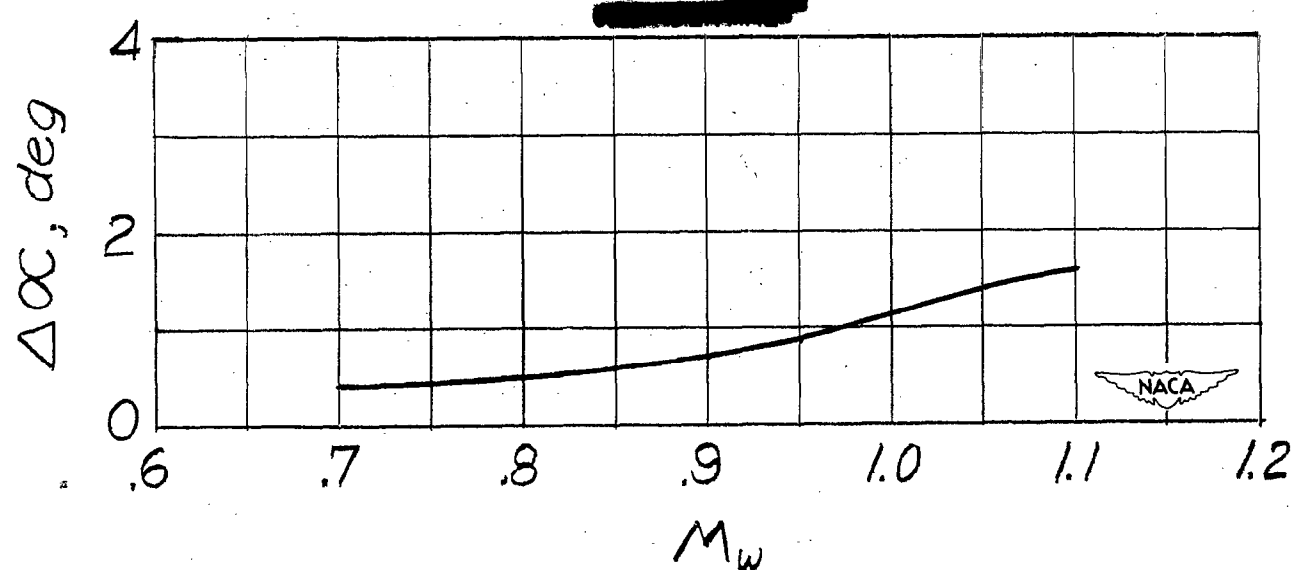


Figure 7.- Variation of difference in flow angle  $\Delta\alpha$  between wing and tail locations on model.

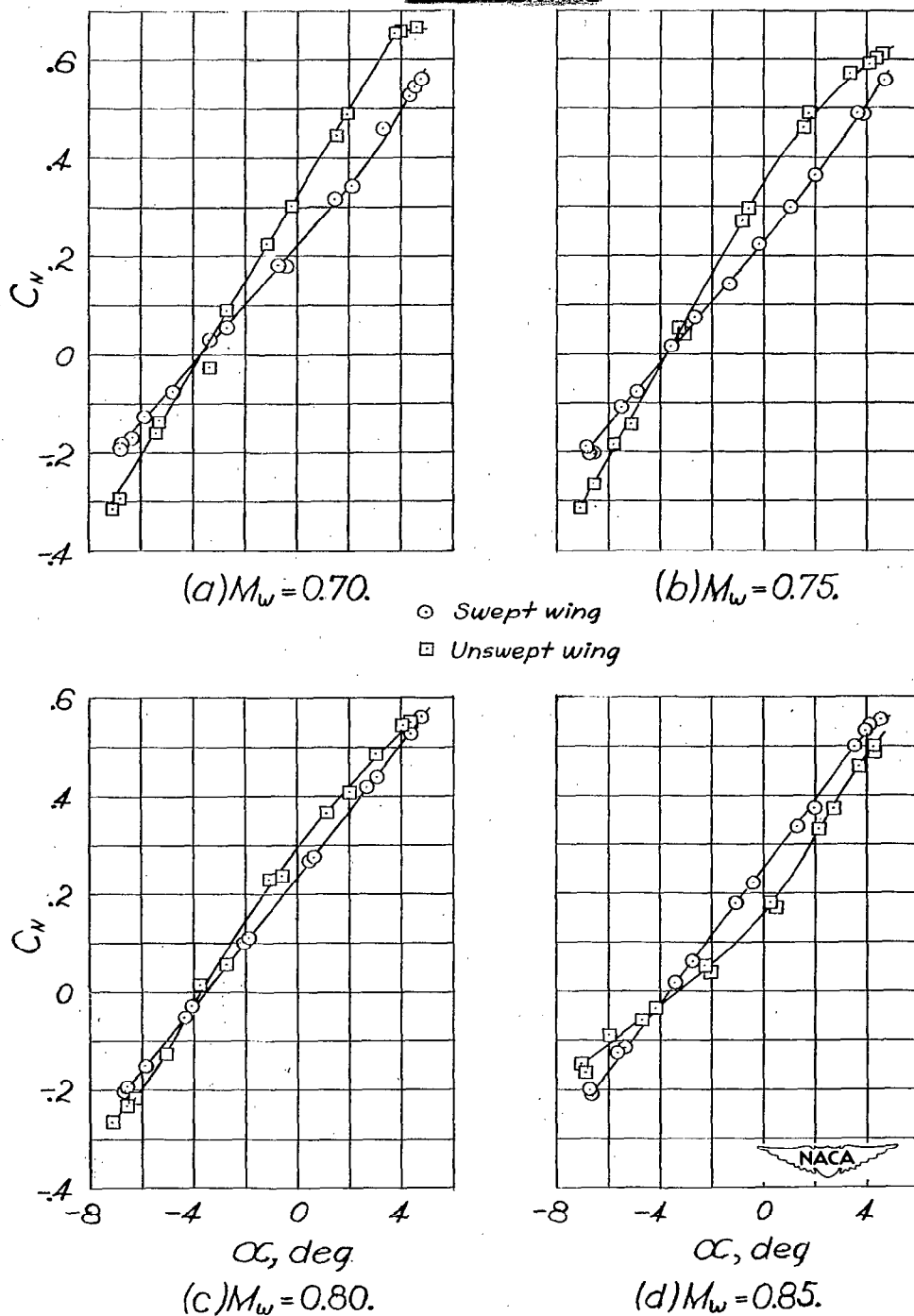


Figure 8.— Variation of normal-force coefficient with angle of attack at several Mach numbers for complete model with each wing.

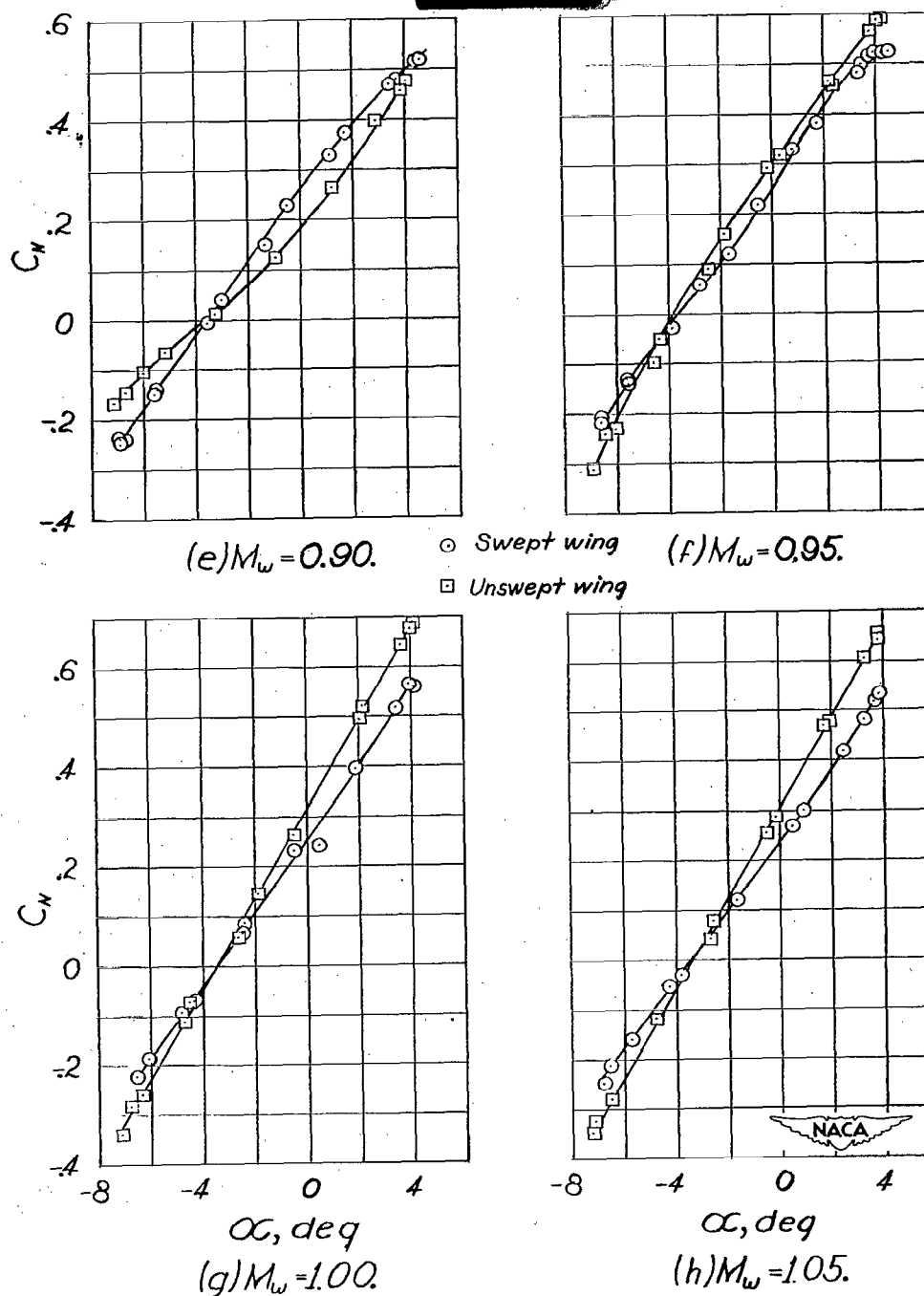


Figure 8.— Concluded.

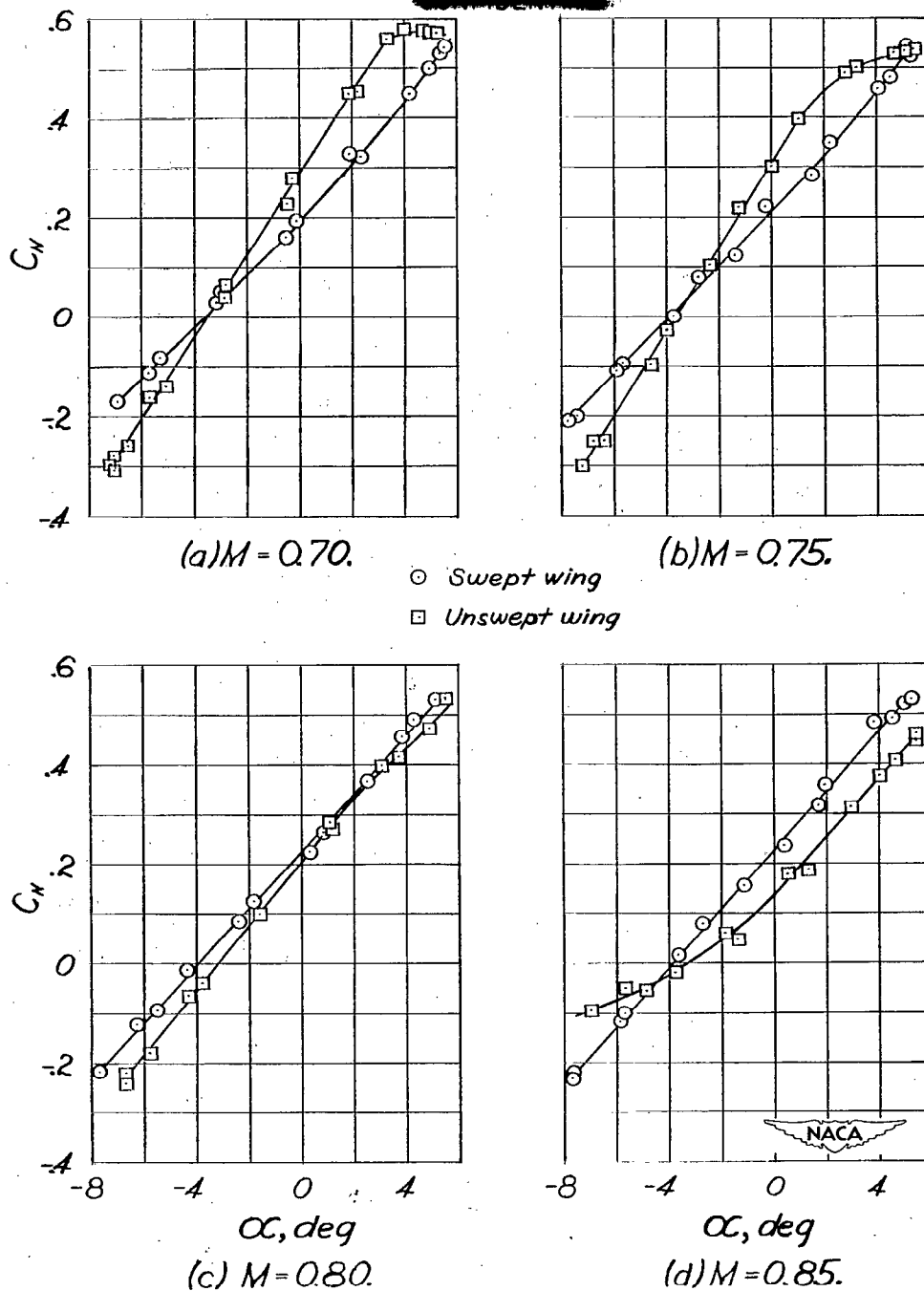


Figure 9.— Variation of normal-force coefficient with angle of attack at several Mach numbers for model with each wing but without empennage.

~~CONFIDENTIAL~~

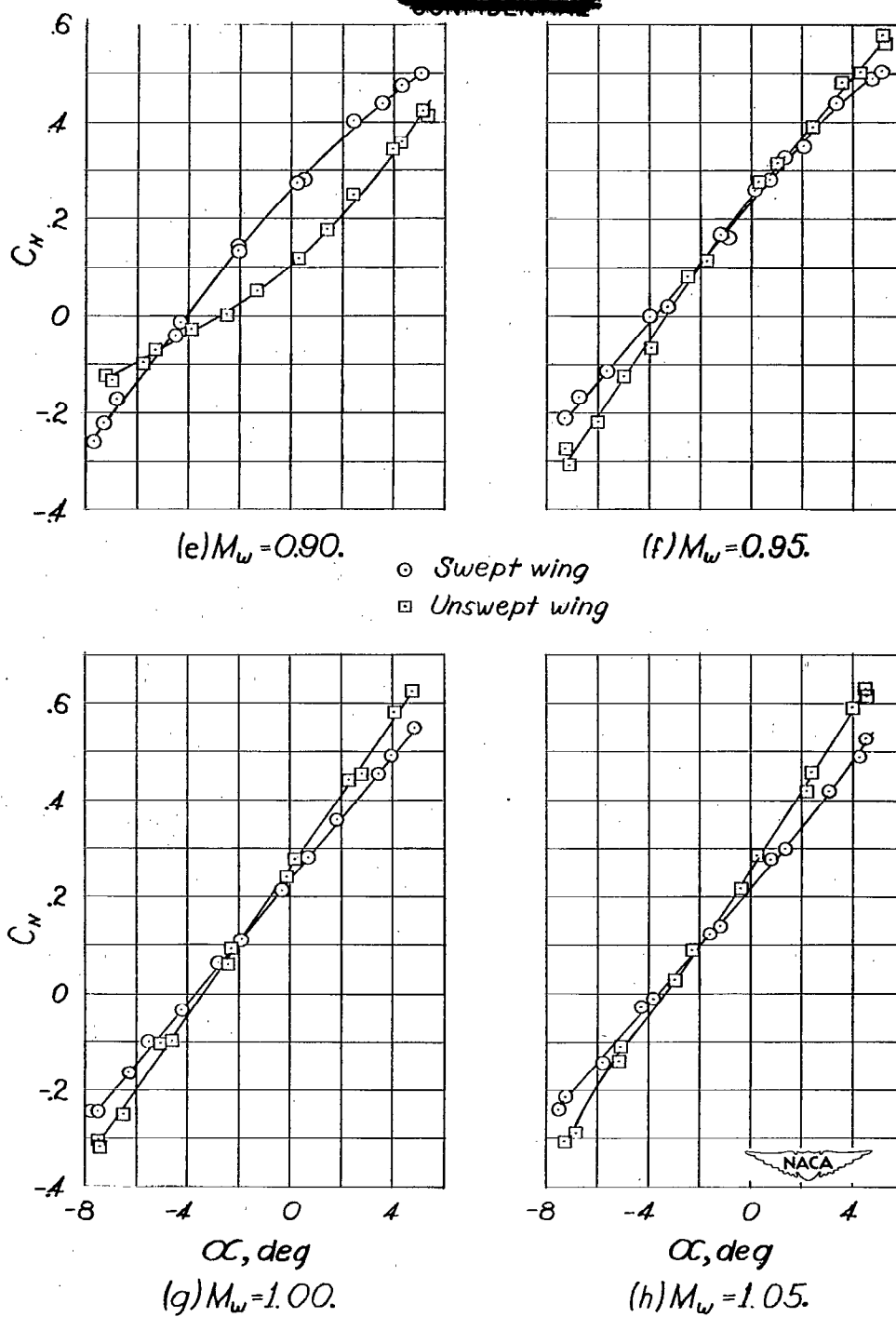
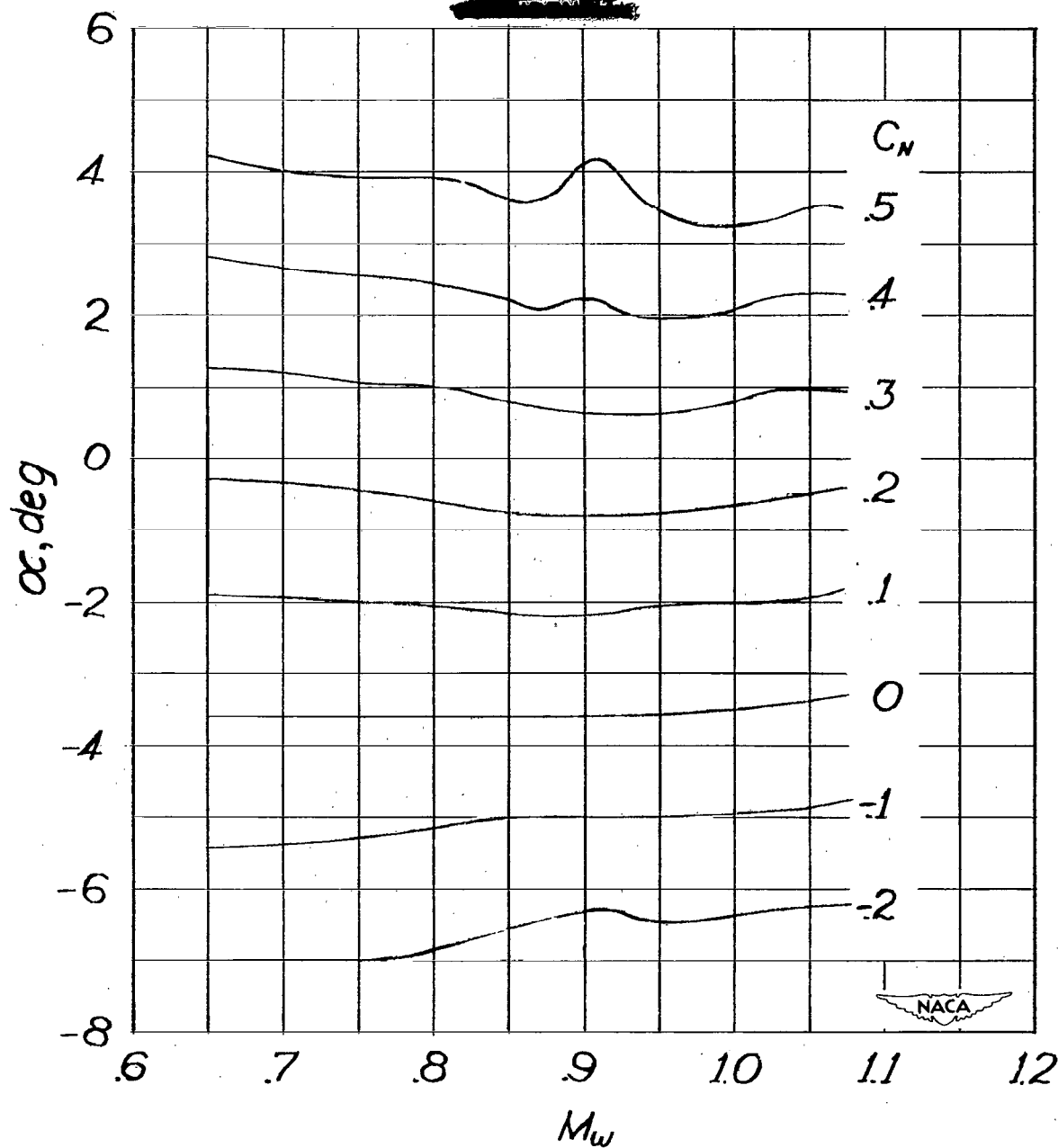
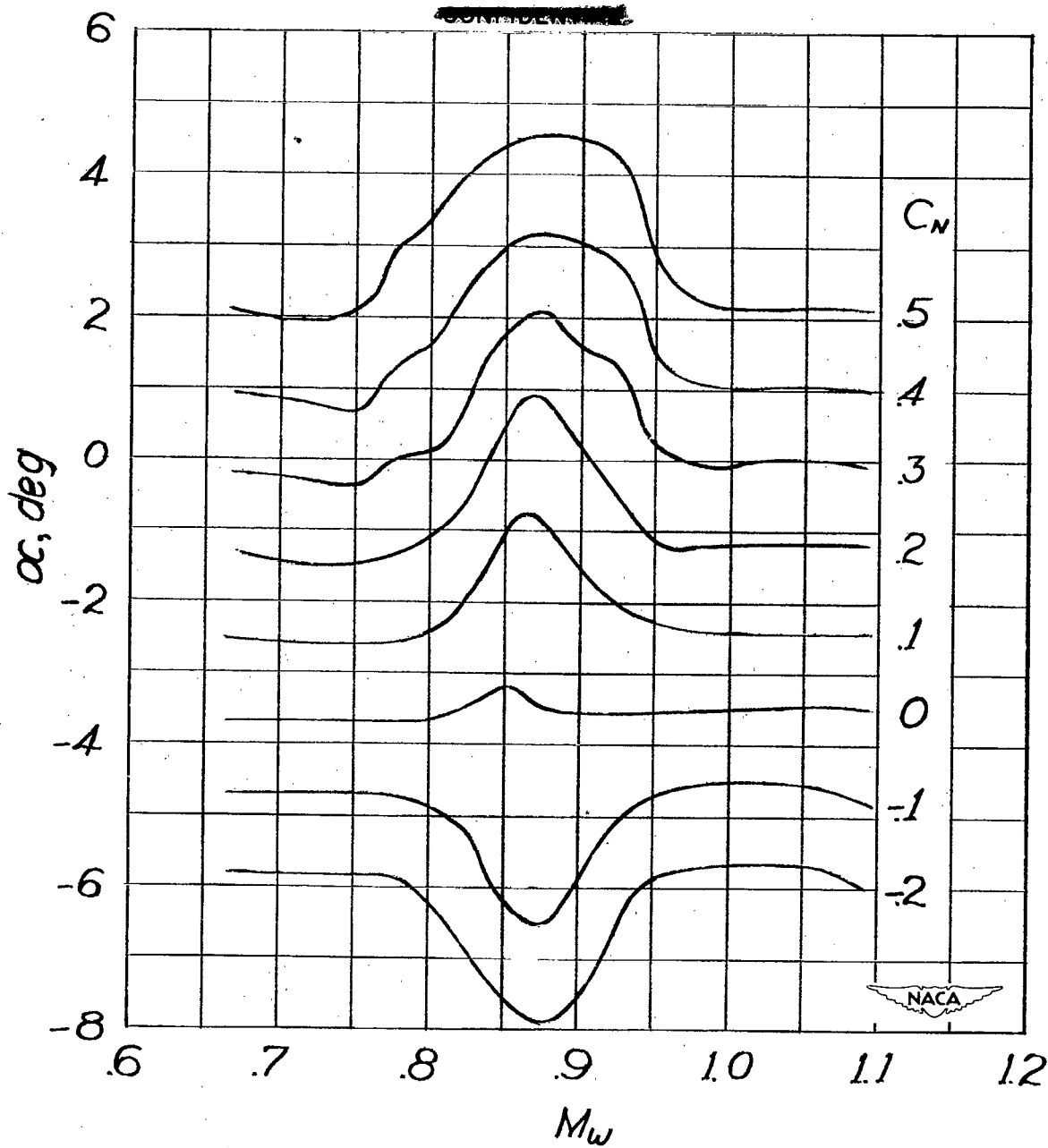


Figure 9.— Concluded.



(a) Complete model with swept wing.

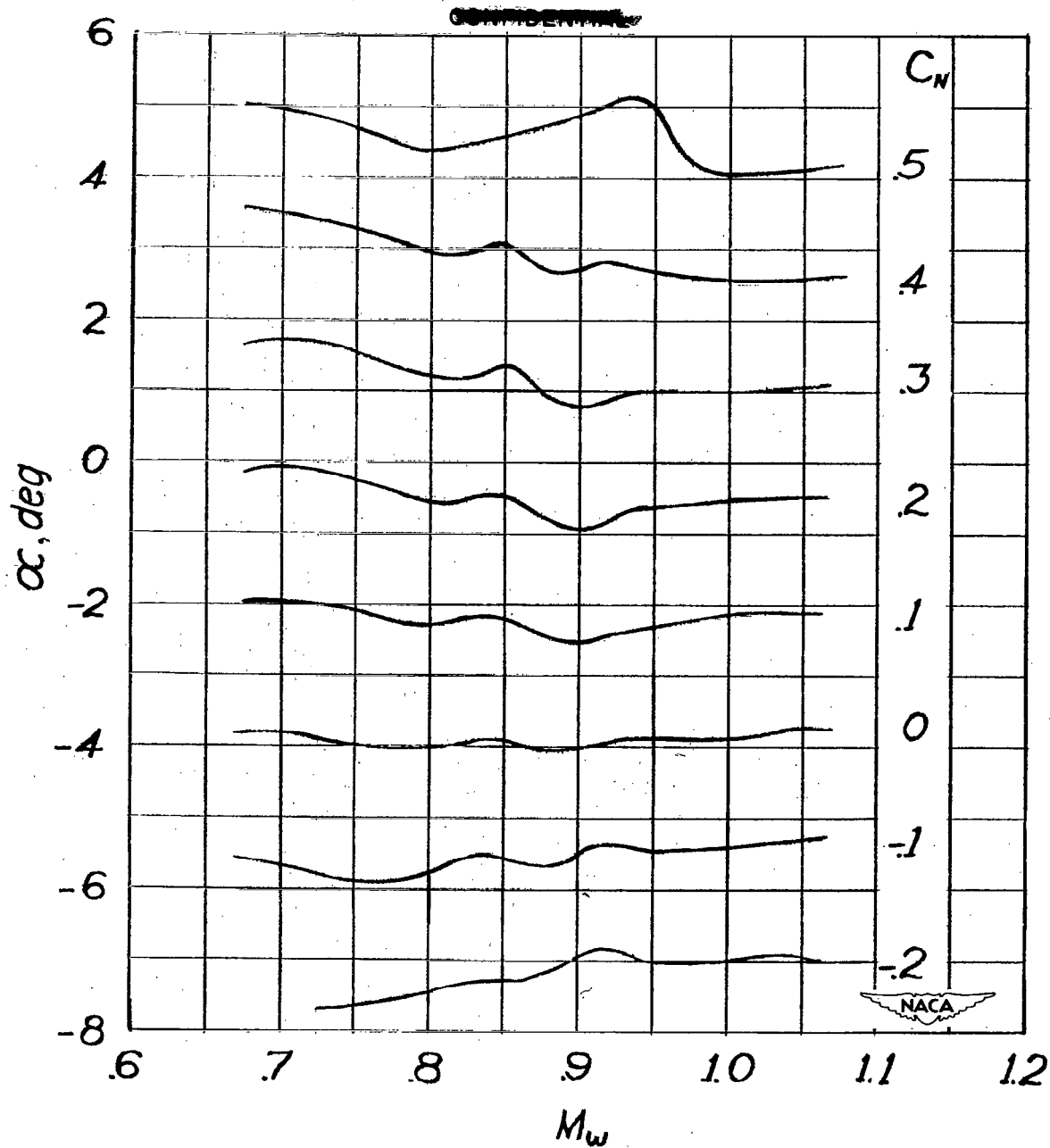
Figure 10.— Variation with Mach number of angle of attack at various normal-force coefficients.



(b) Complete model with straight wing.

Figure 10.— Continued.

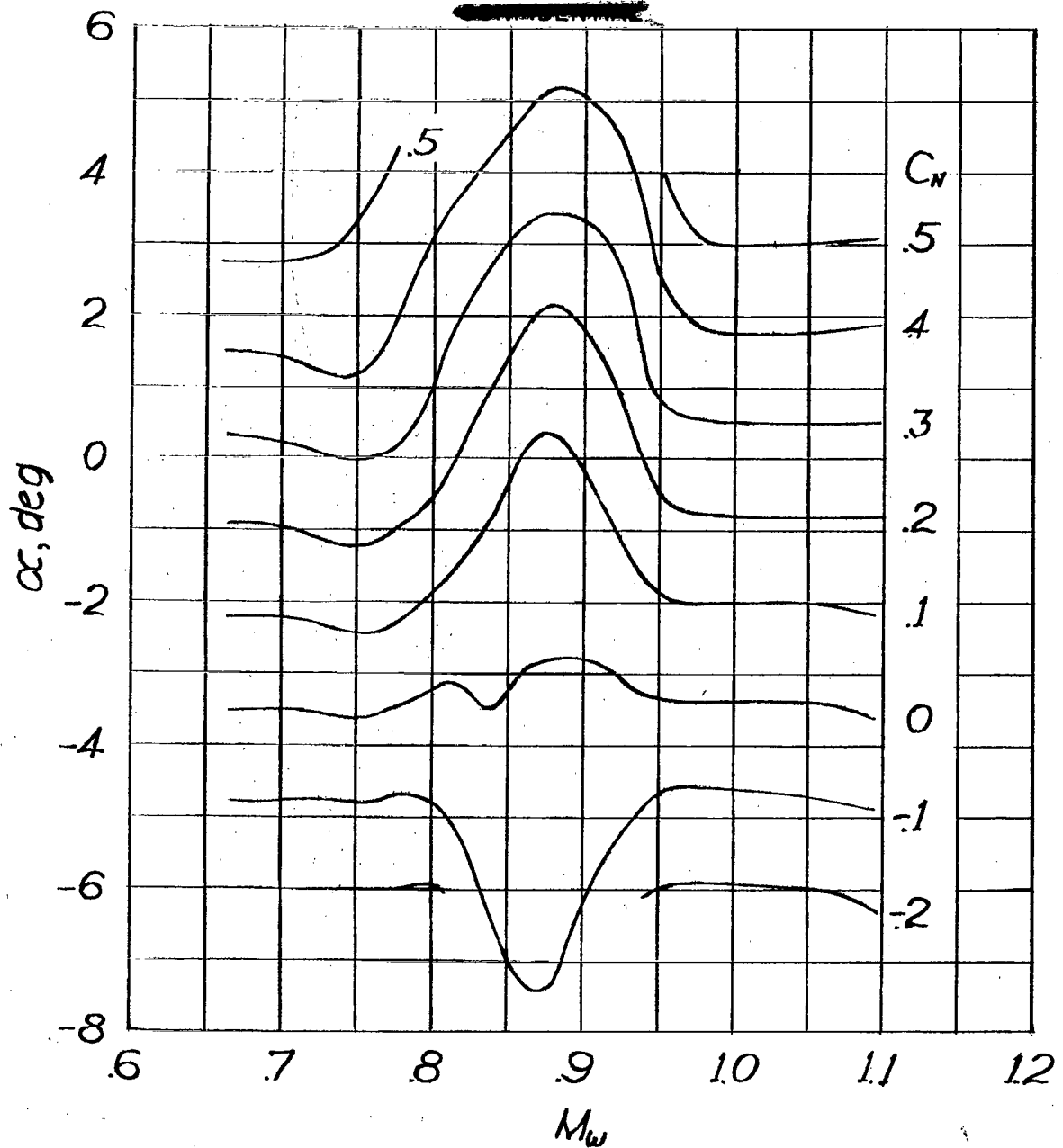
~~CONFIDENTIAL~~



(c) Model less empennage with swept wing.

Figure 10:- Continued.

~~CONFIDENTIAL~~



(d) Model less empennage with straight wing.

Figure 10.- Concluded.

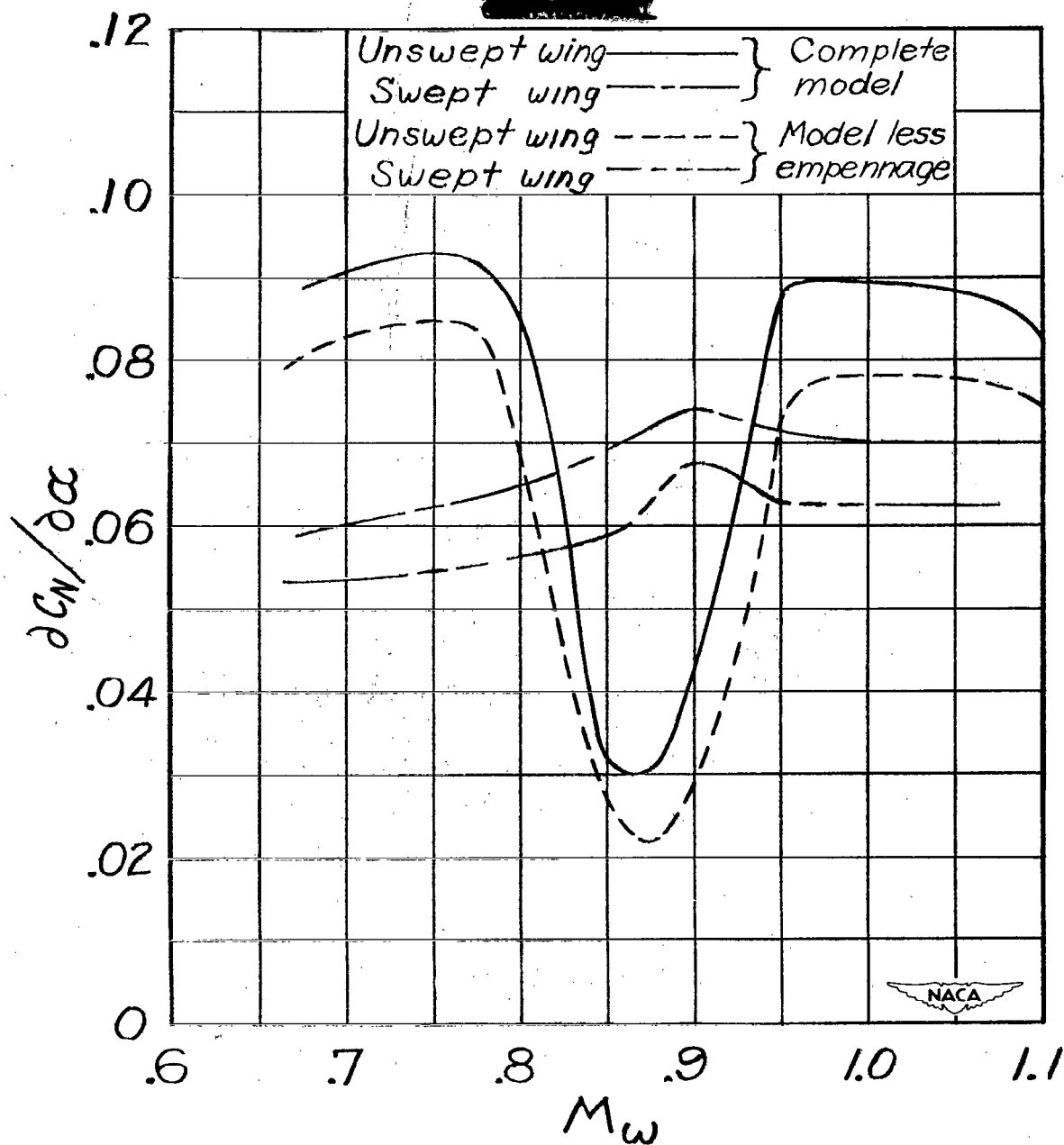


Figure 11.— Variation with Mach number of rate of change of normal-force coefficient with angle of attack for the complete model with each wing both with and without empennage.  $C_N = 0$ .

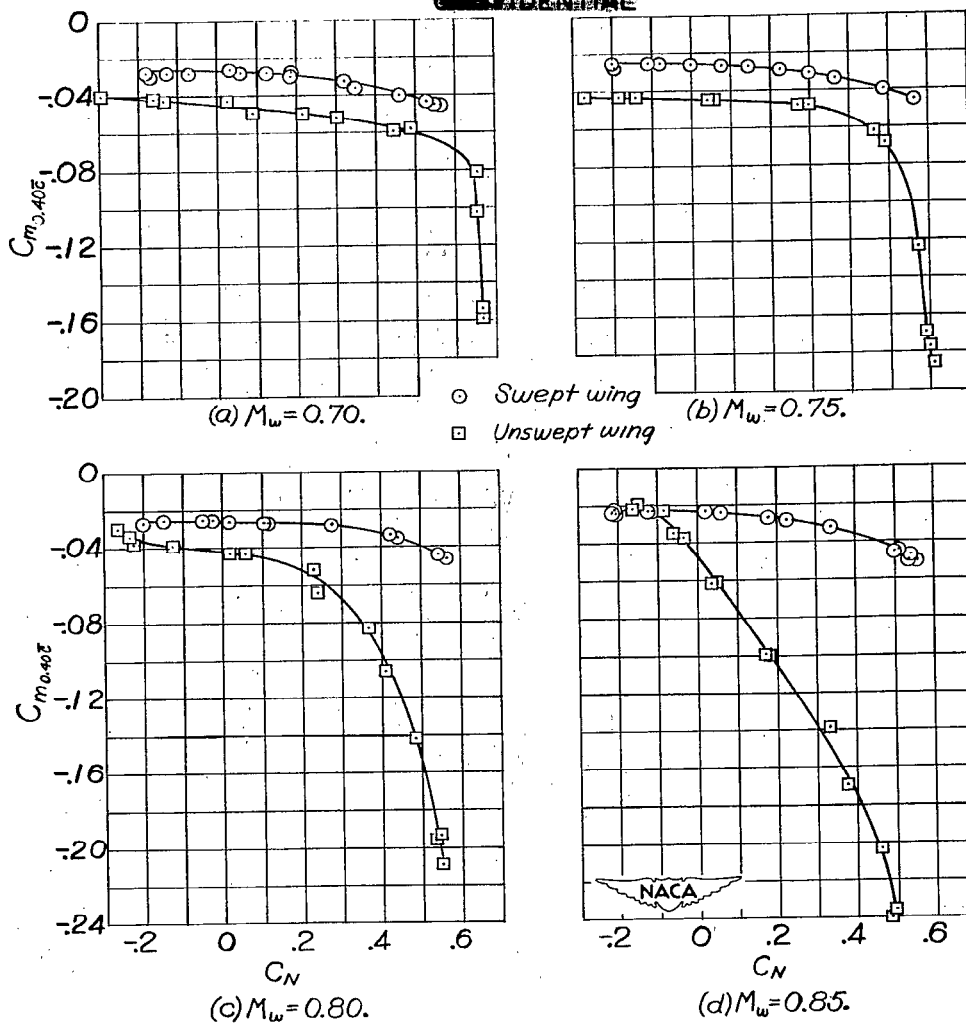


Figure 12.— Variation of pitching-moment coefficient with normal-force coefficient at several Mach numbers for complete model with each wing.

~~CONFIDENTIAL~~

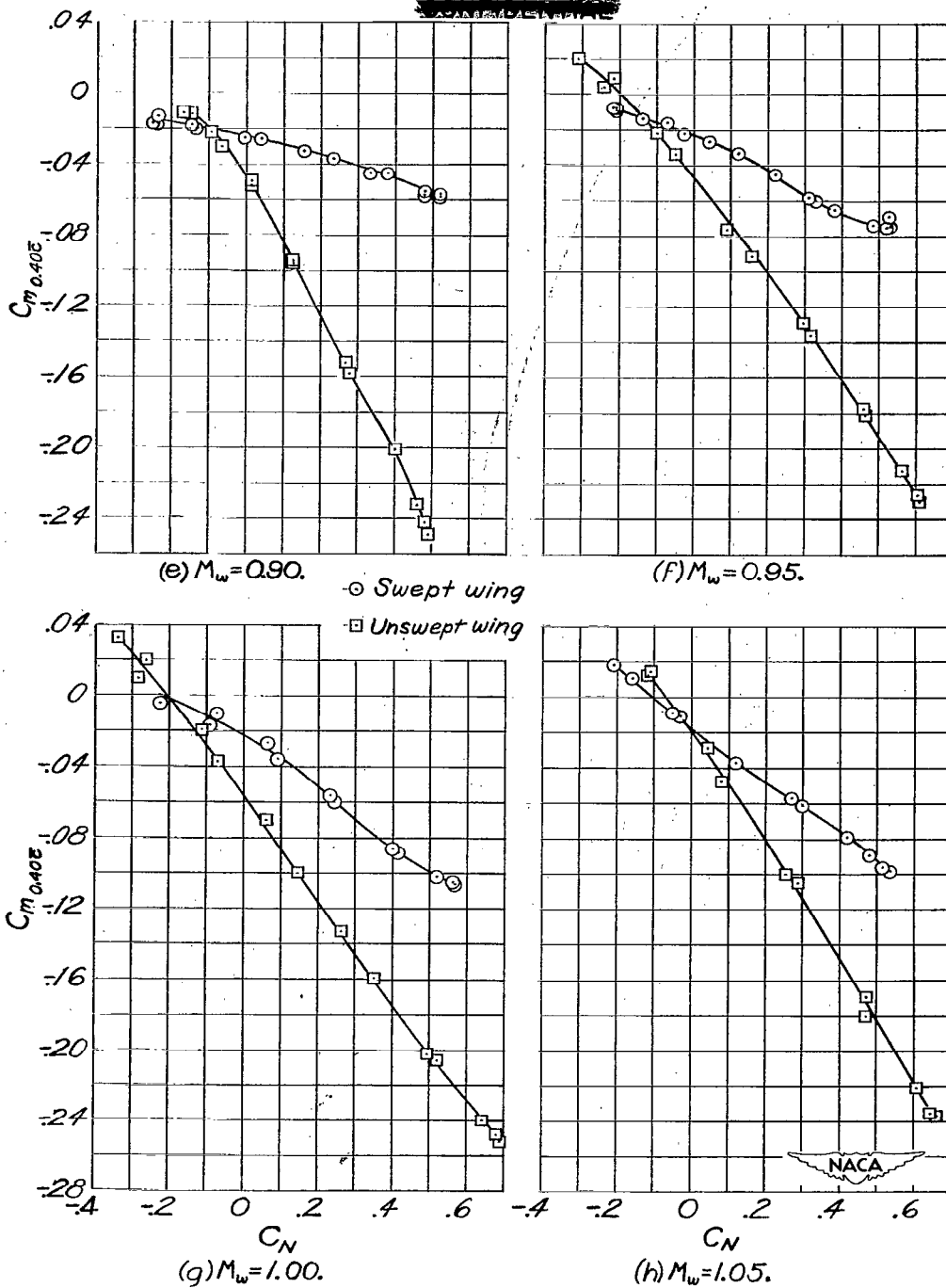


Figure 12.— Concluded.

~~CONFIDENTIAL~~

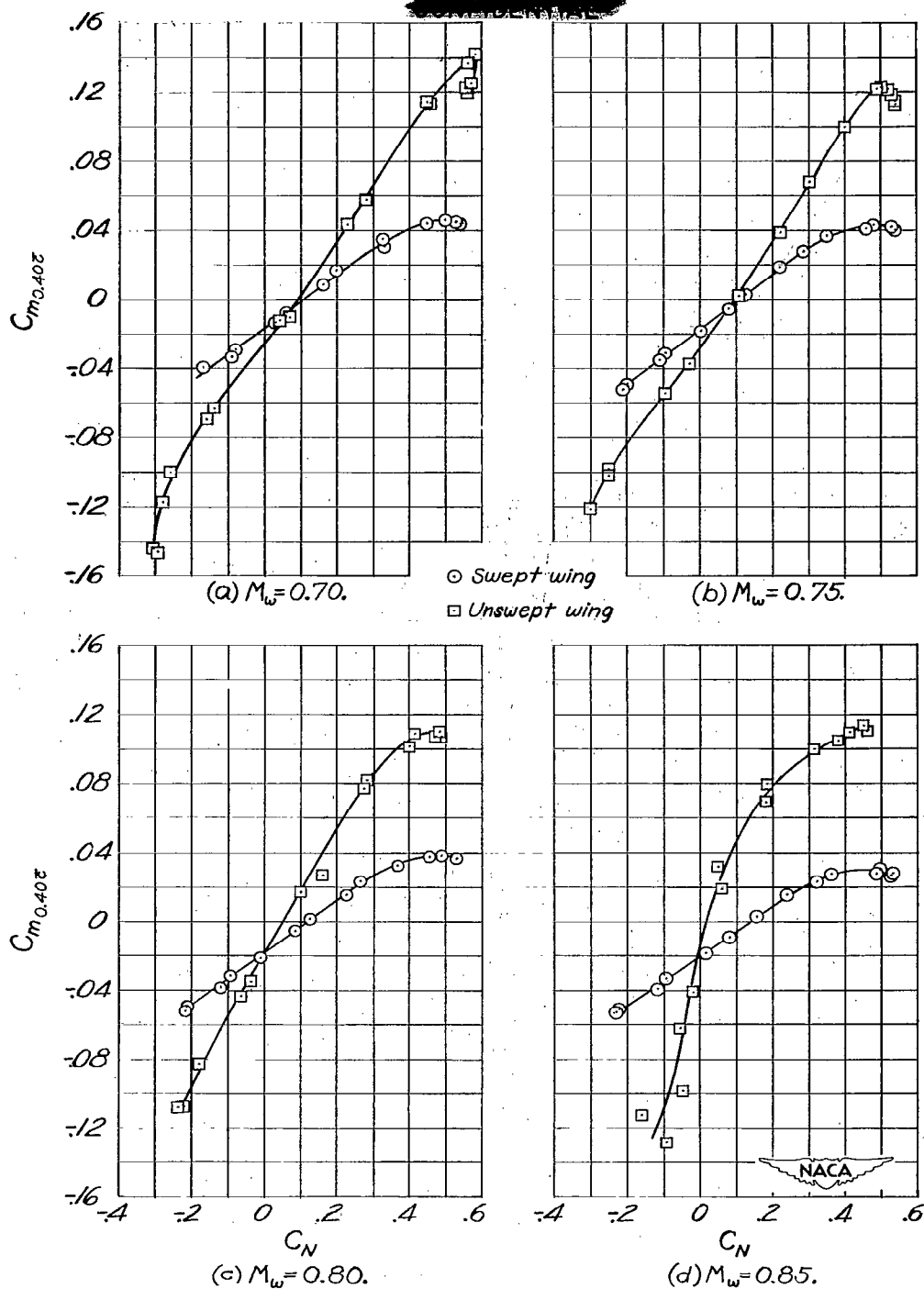


Figure 13.— Variation of pitching-moment coefficient with normal-force coefficient at several Mach numbers for the model with each wing but without empennage.

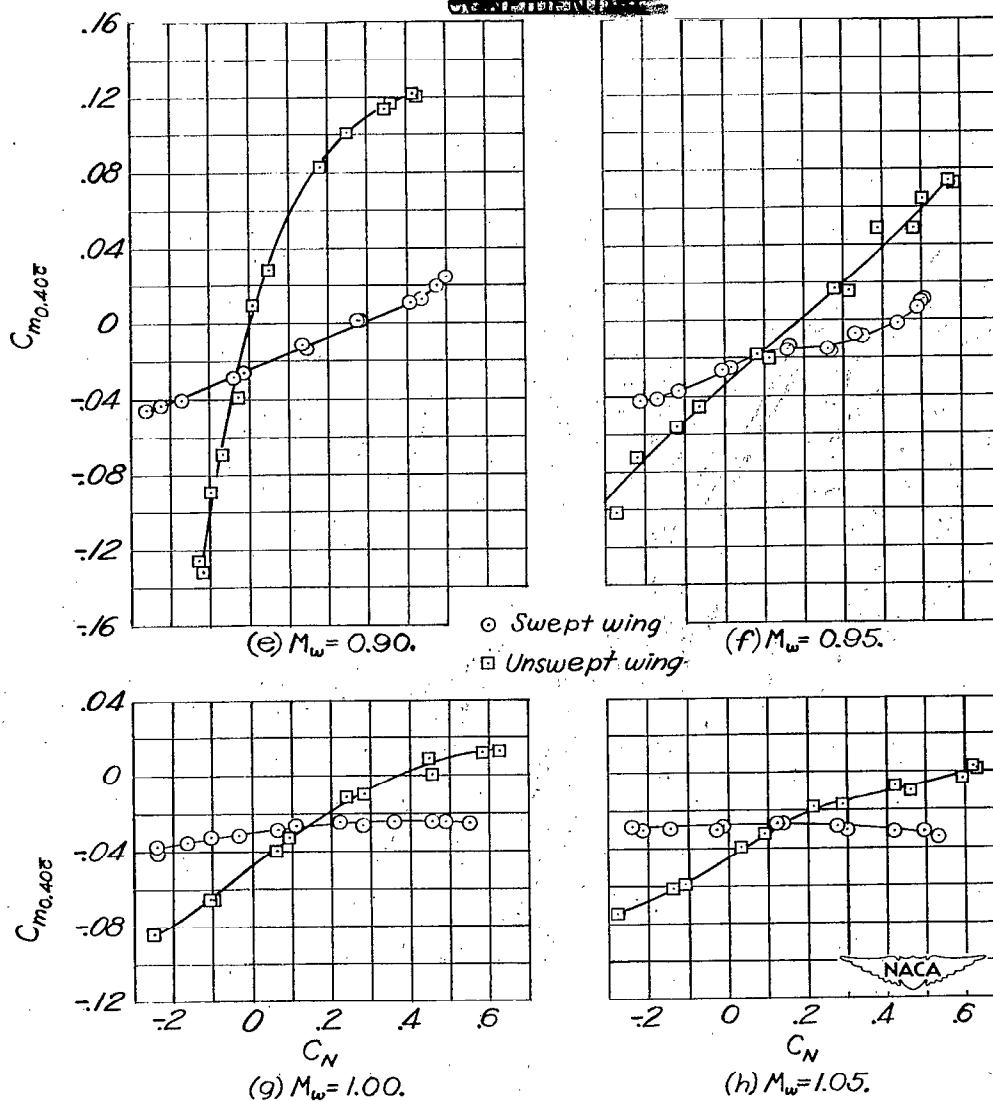
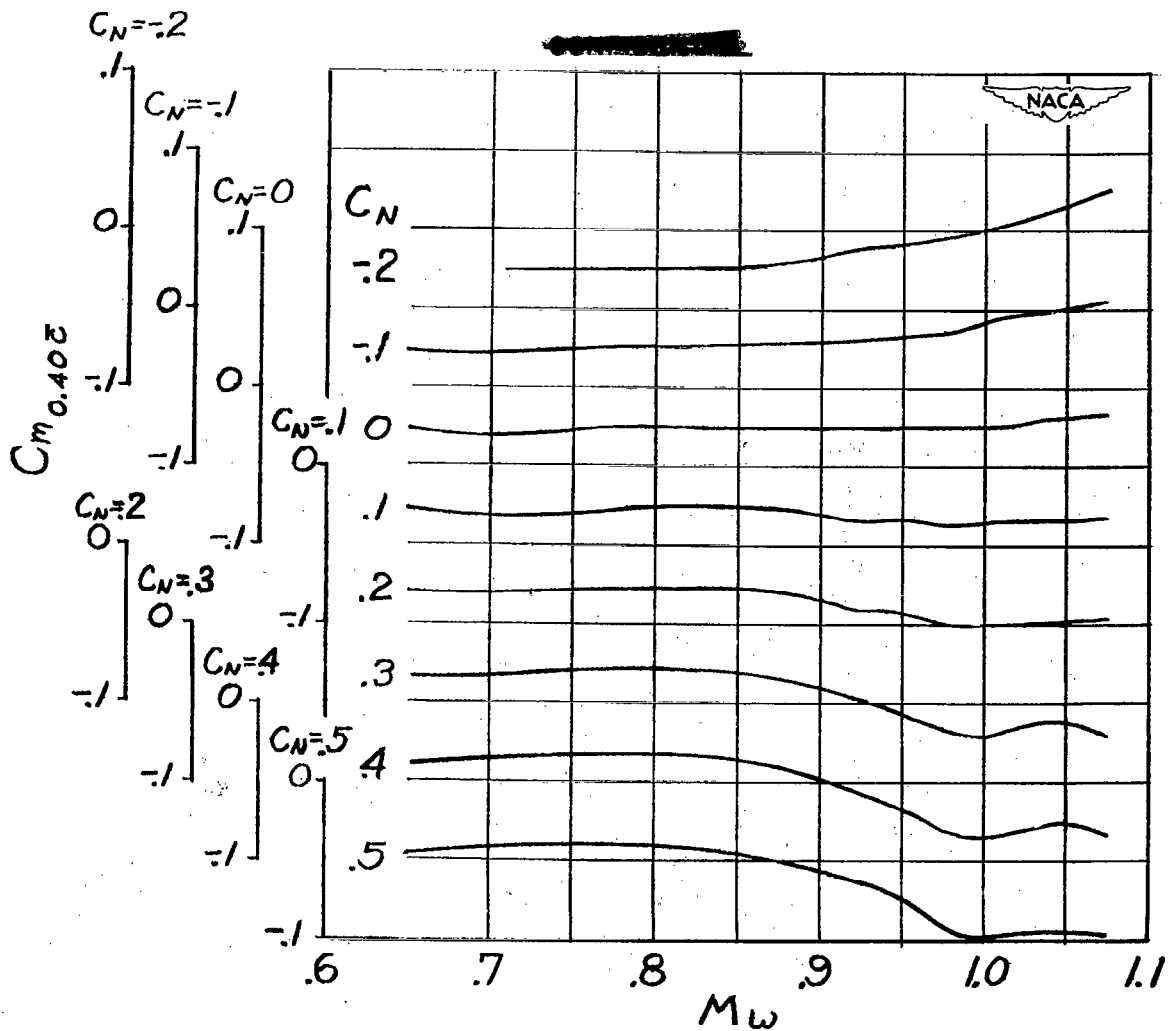


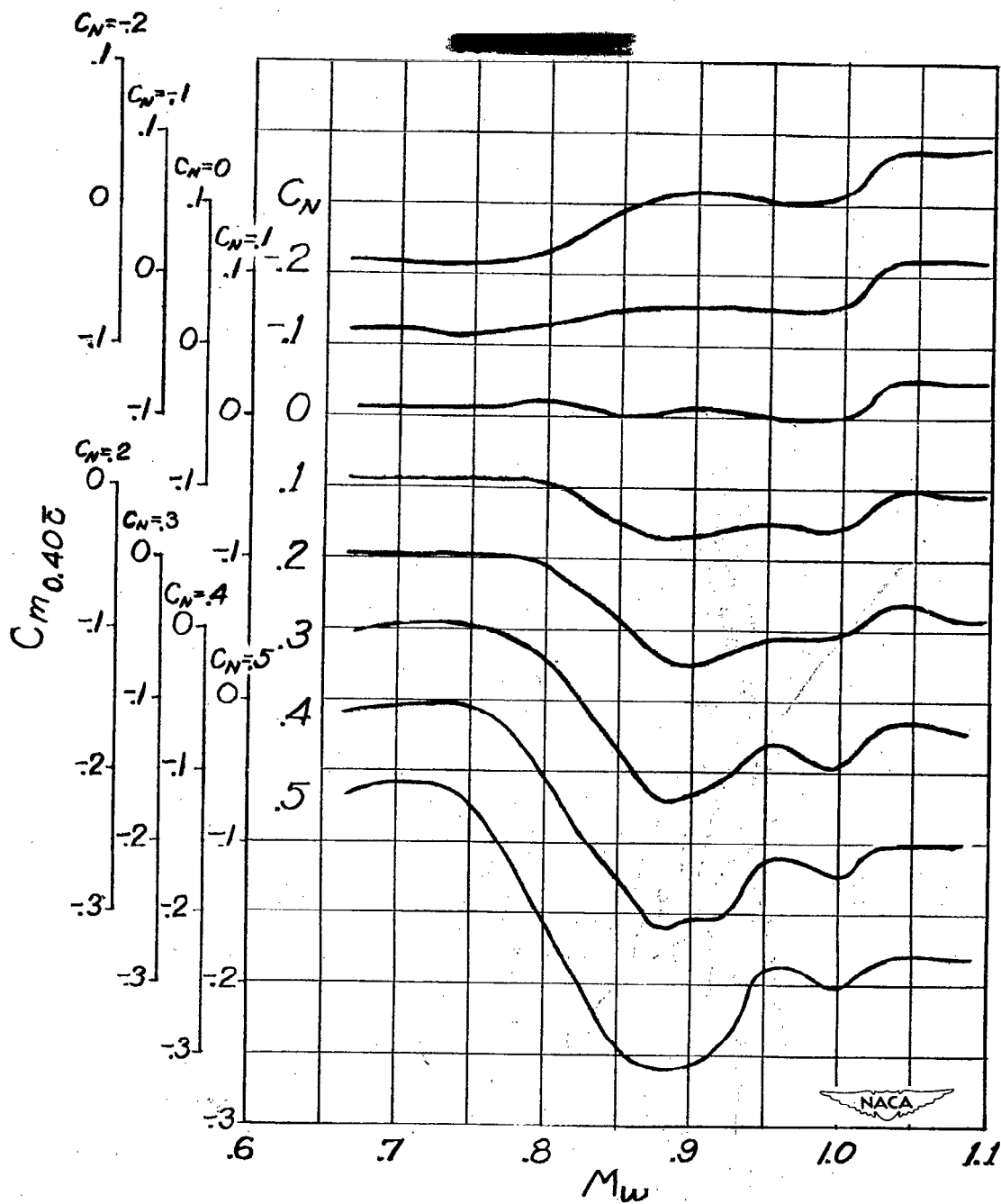
Figure 13.- Concluded.



(a) Complete model with sweptback wing.

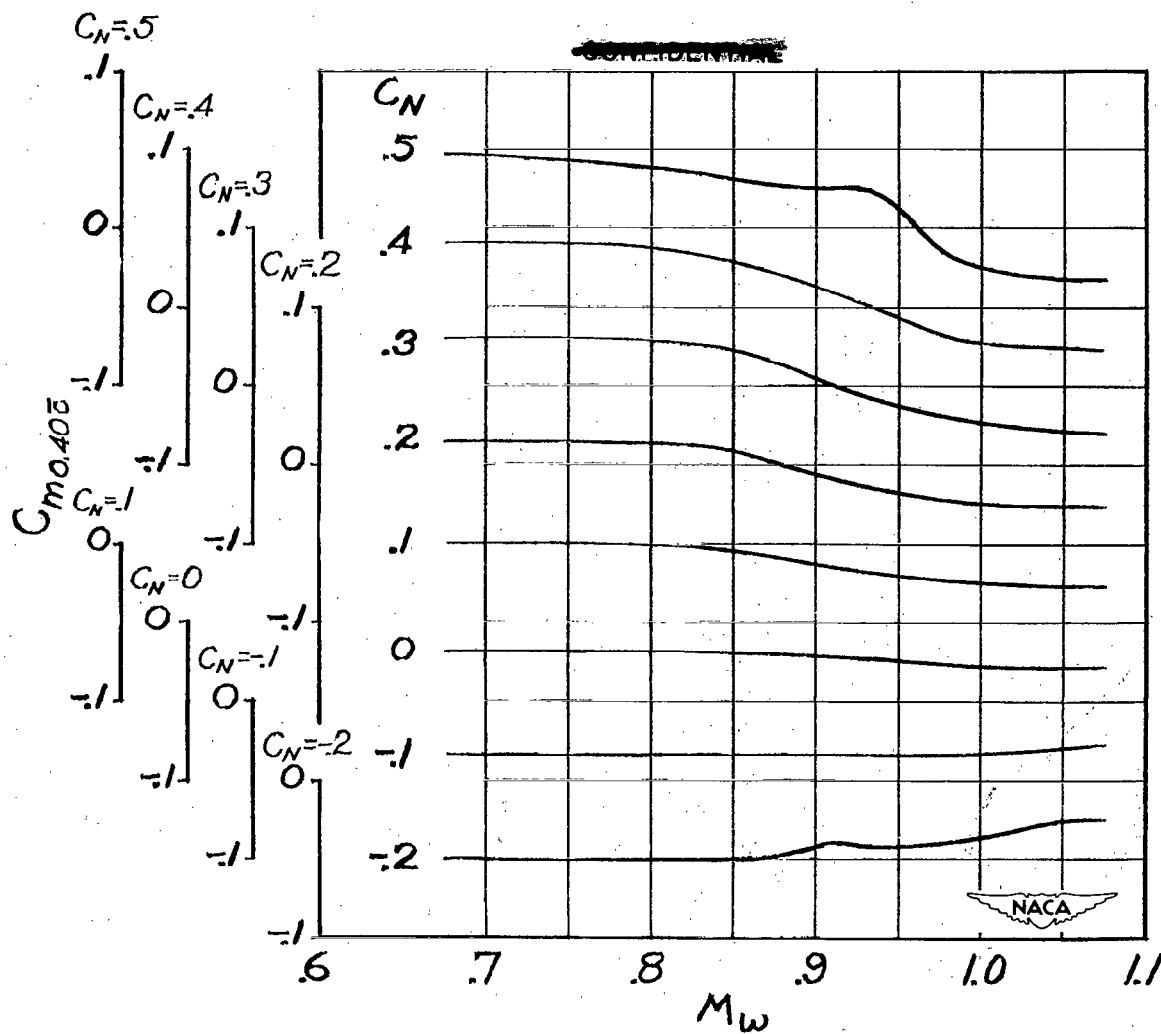
Figure 14.— Variation with Mach number of pitching-moment coefficient at several normal-force coefficients.

~~CONFIDENTIAL~~



(b) Complete model with straight wing.

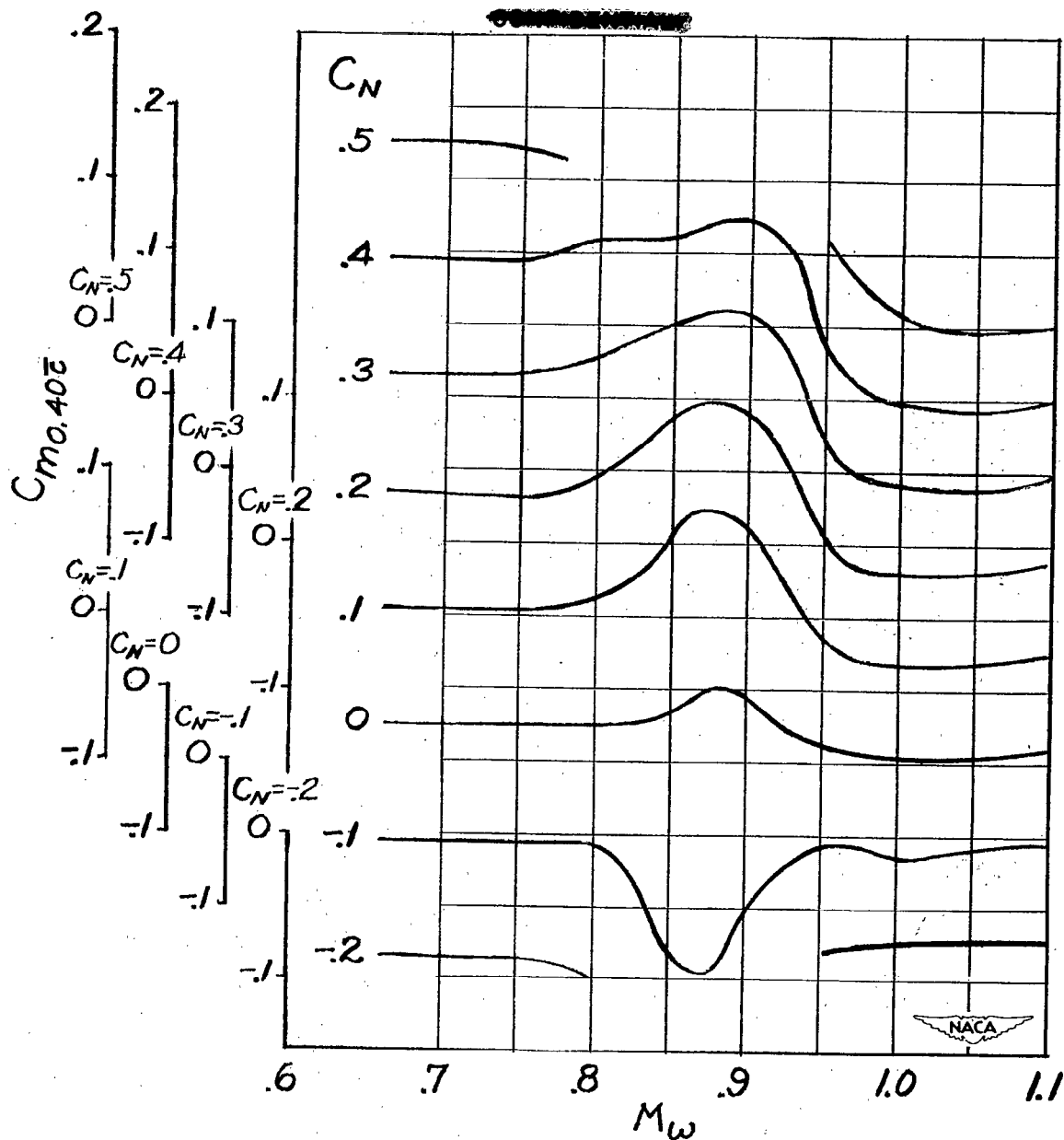
Figure 14.- Continued.



(c) Model with swept wing but without empennage.

Figure 14.- Continued.

~~CONFIDENTIAL~~



(d) Model with straight wing but without empennage.

Figure 14.- Concluded.

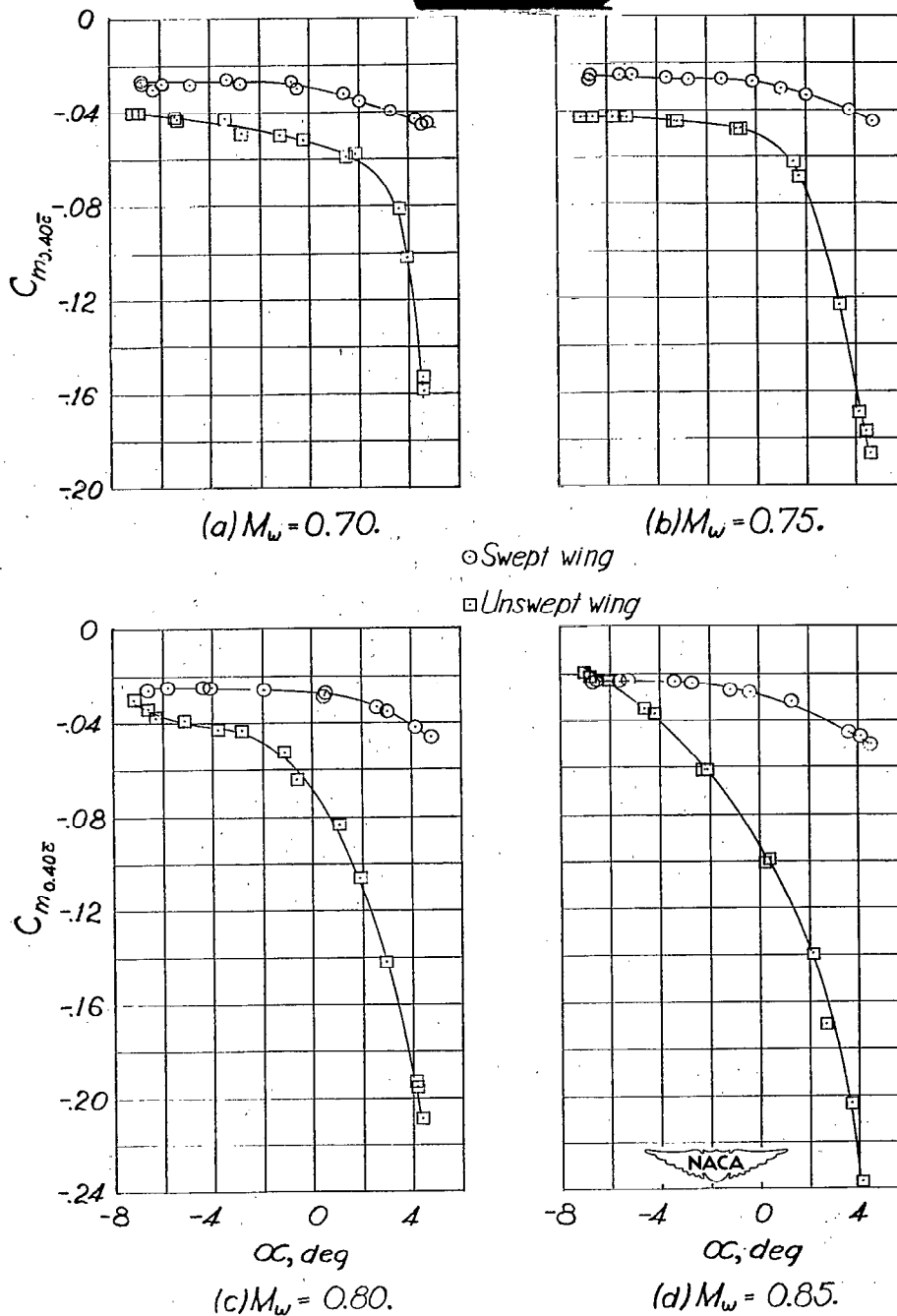


Figure 15.— Variation of pitching-moment coefficient with angle of attack at several Mach numbers for the complete model with each wing.

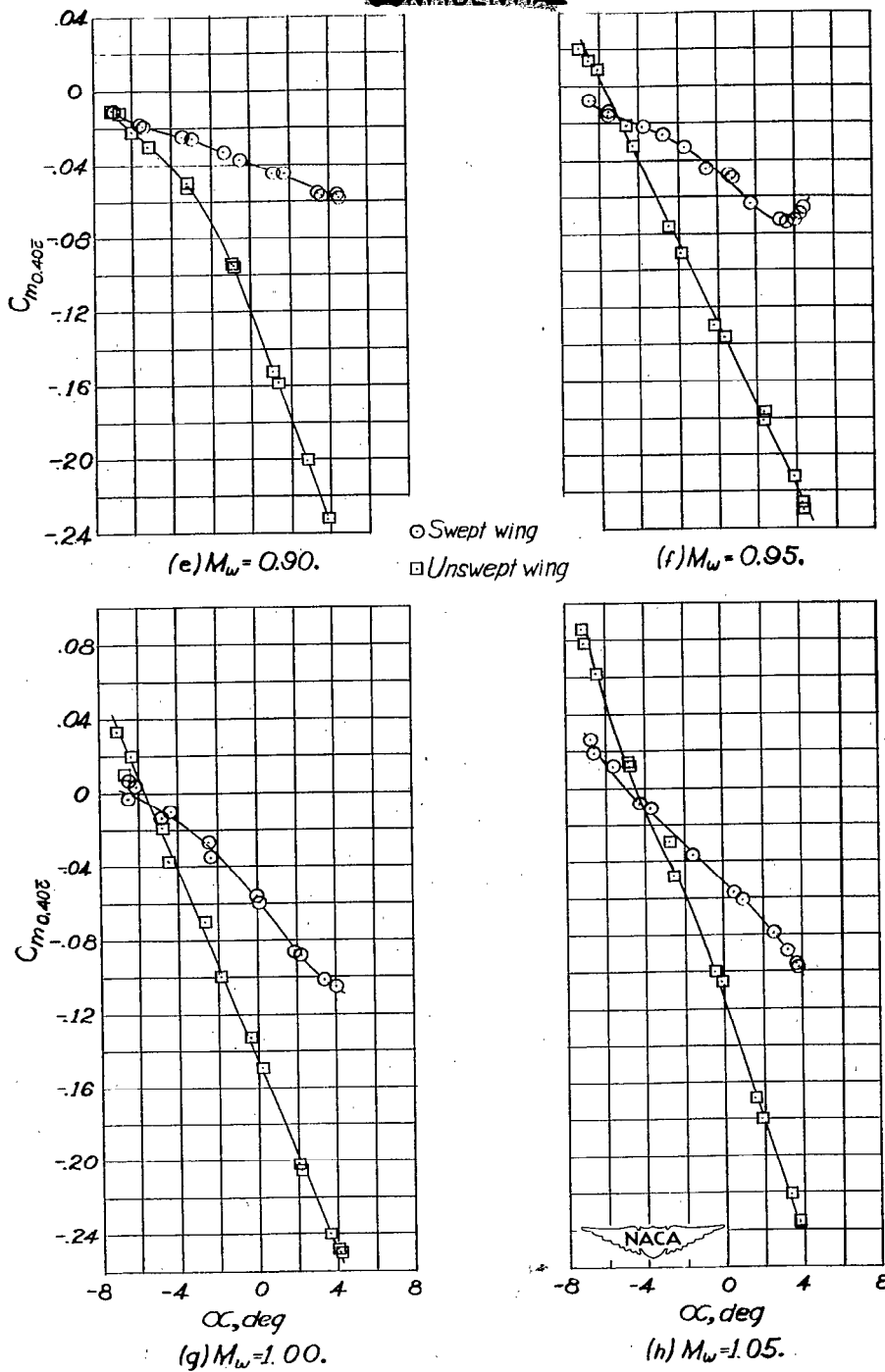


Figure 15.- Concluded.

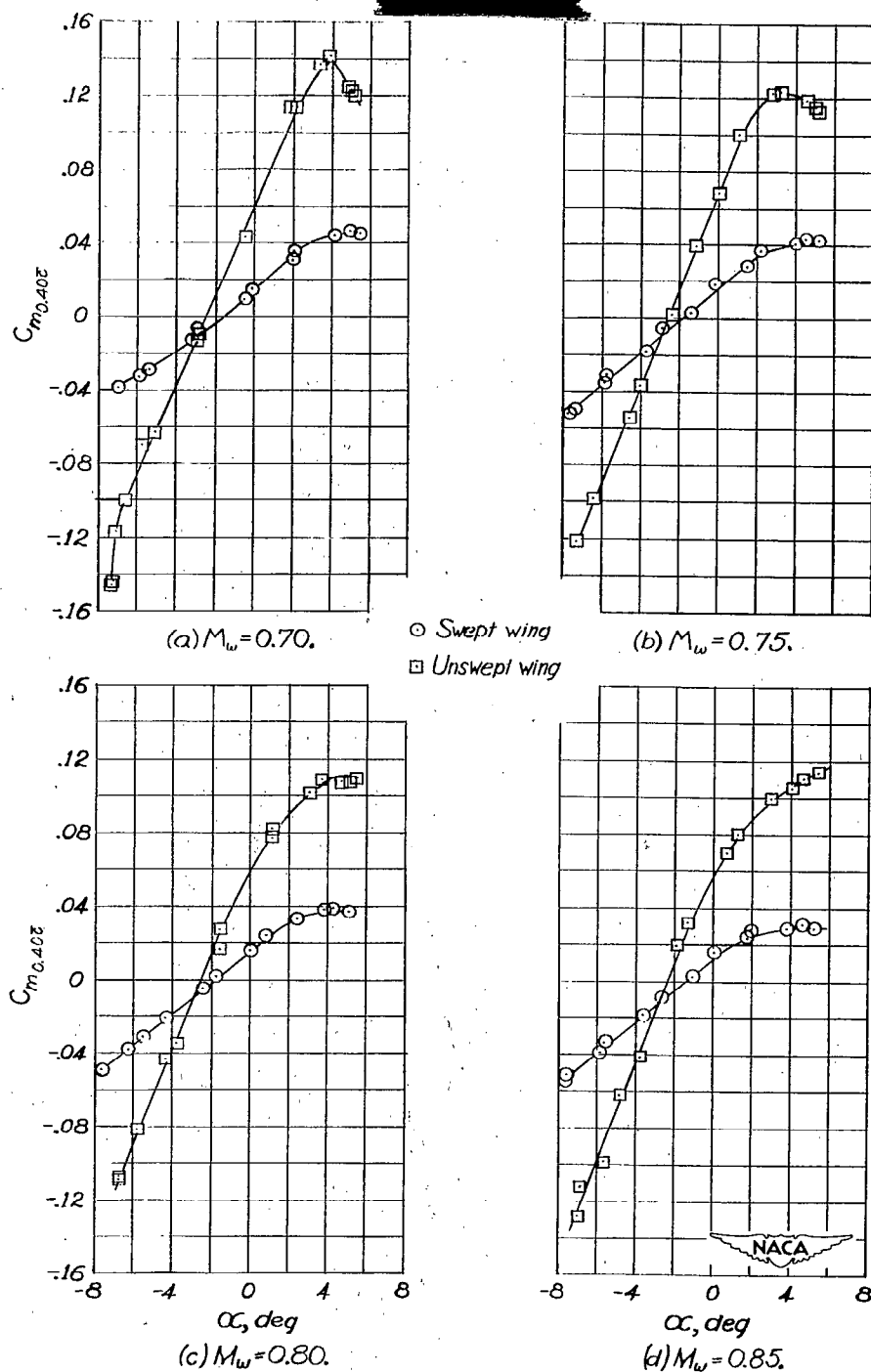
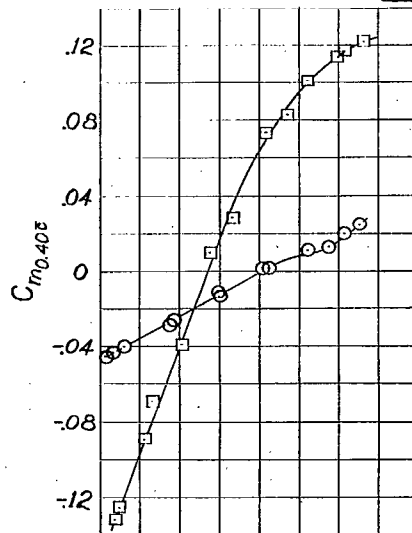
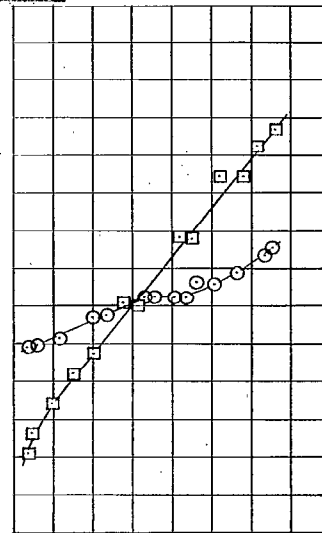


Figure 16.— Variation of pitching-moment coefficient with angle of attack at several Mach numbers for the model with each wing, but without the empennage.



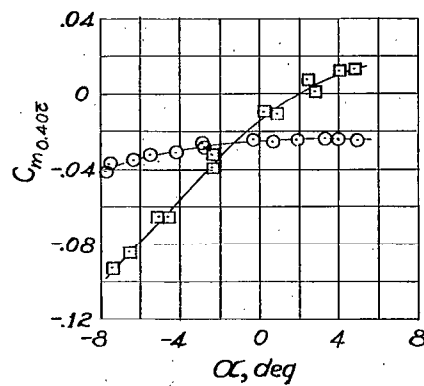
(e)  $M_w = 0.90$ .



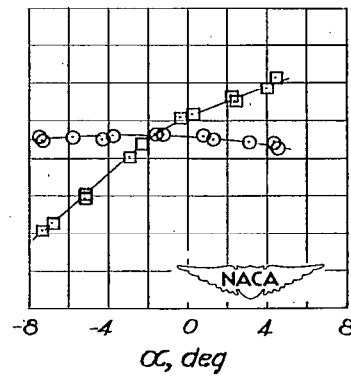
(f)  $M_w = 0.95$ .

○ Swept wing

□ Unswept wing



(g)  $M_w = 1.00$ .



(h)  $M_w = 1.05$ .

Figure 16.— Concluded.

~~CONFIDENTIAL~~

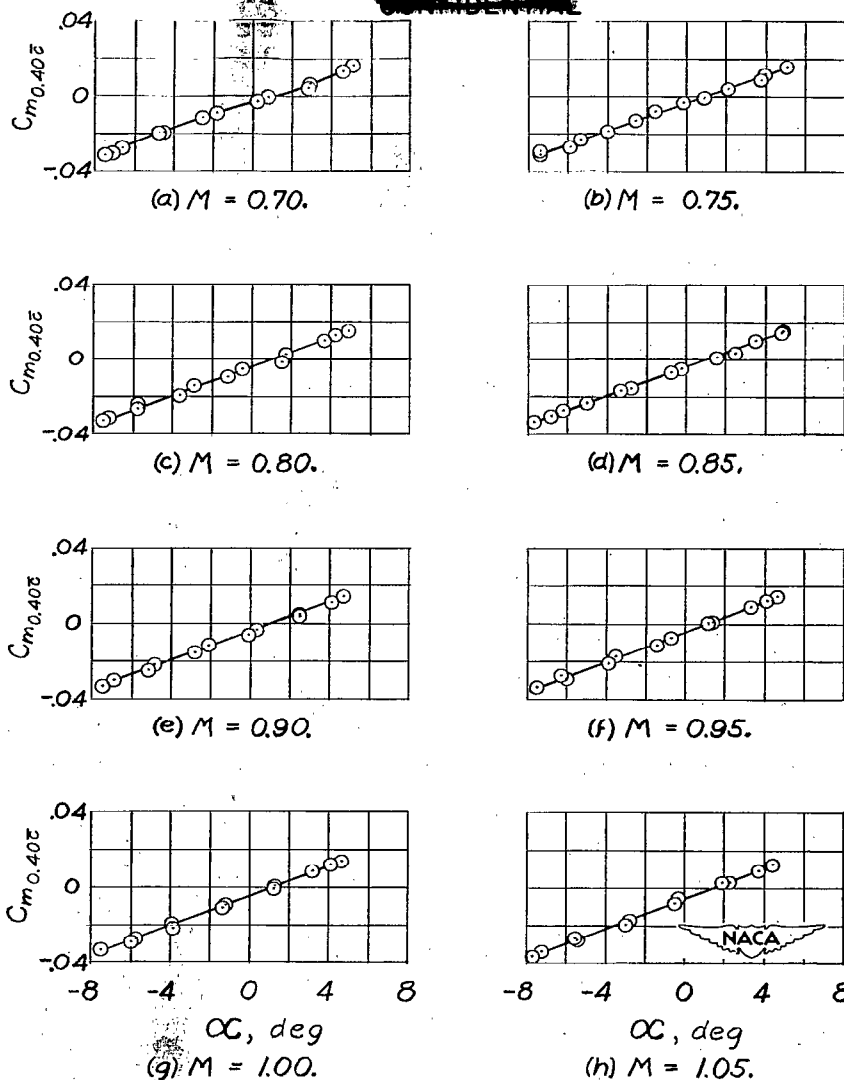


Figure 17.— Variation of pitching-moment coefficient with angle of attack at several Mach numbers for the semispan fuselage alone.

~~CONFIDENTIAL~~

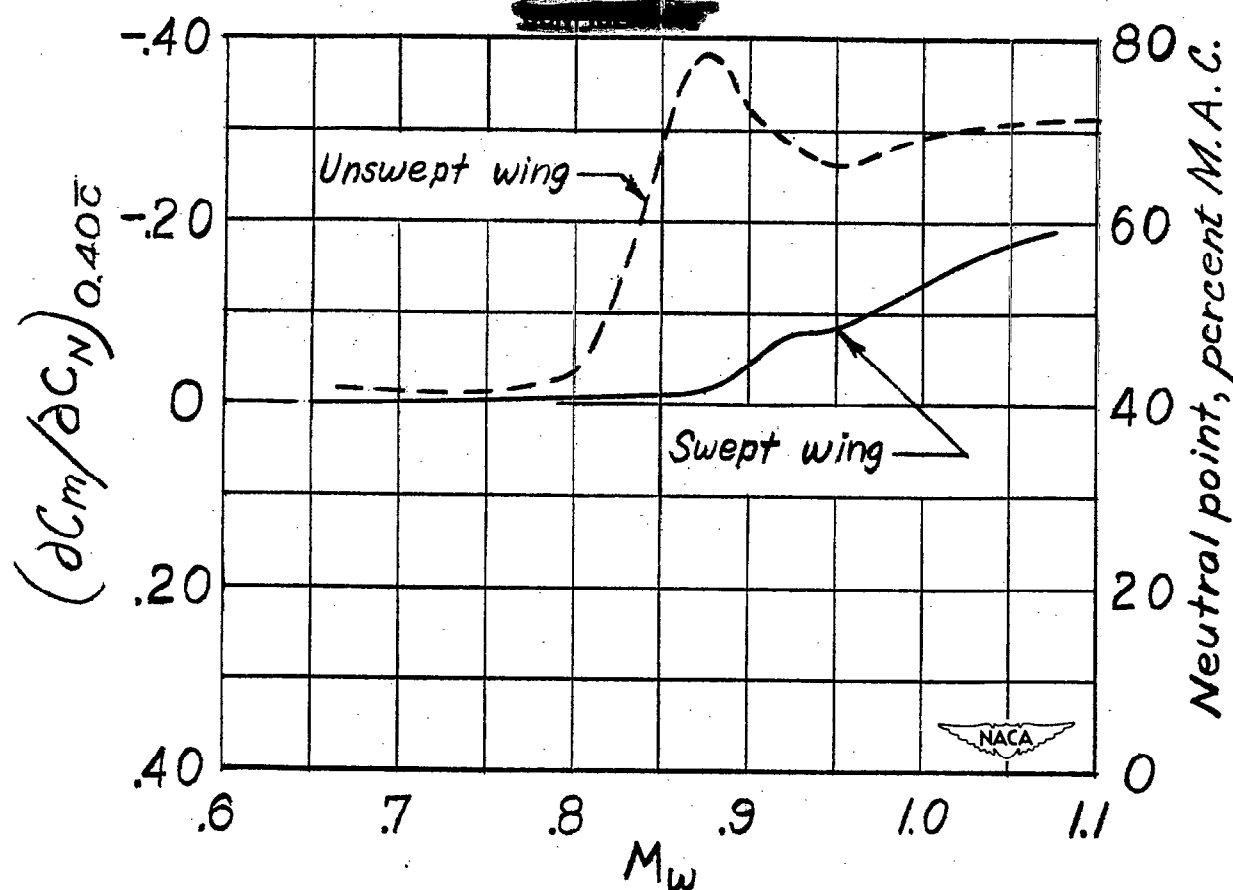
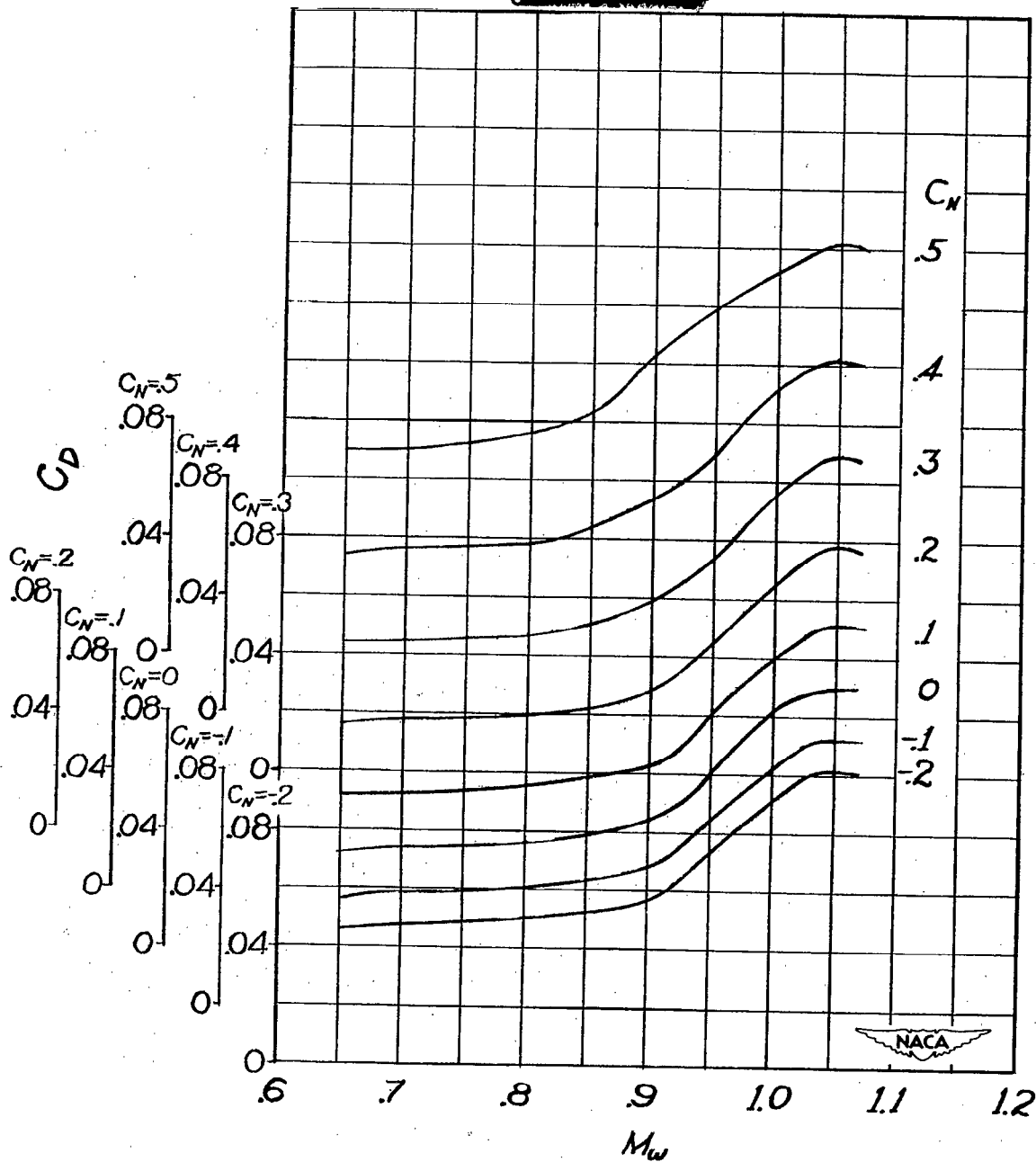


Figure 18.— Variation with Mach number of rate of change of pitching-moment coefficient with normal-force coefficient  $\frac{\partial C_m}{\partial C_N}$  for complete model with both straight and swept wing.  $C_N = 0$ .

~~CONFIDENTIAL~~

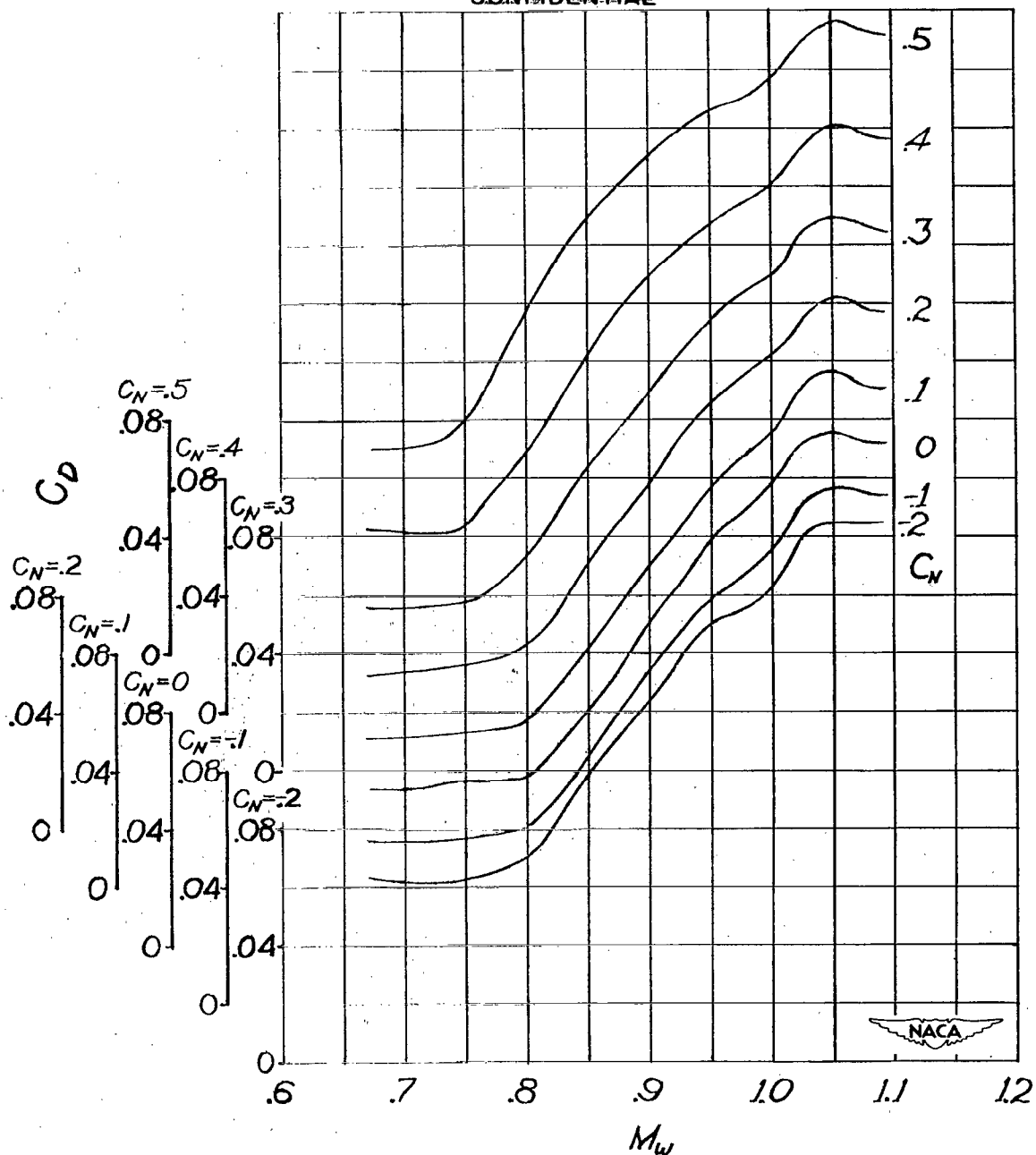


(a) Complete model with swept wing.

Figure 19.— Variation with Mach number of drag coefficient for several normal-force coefficients.

CONFIDENTIAL

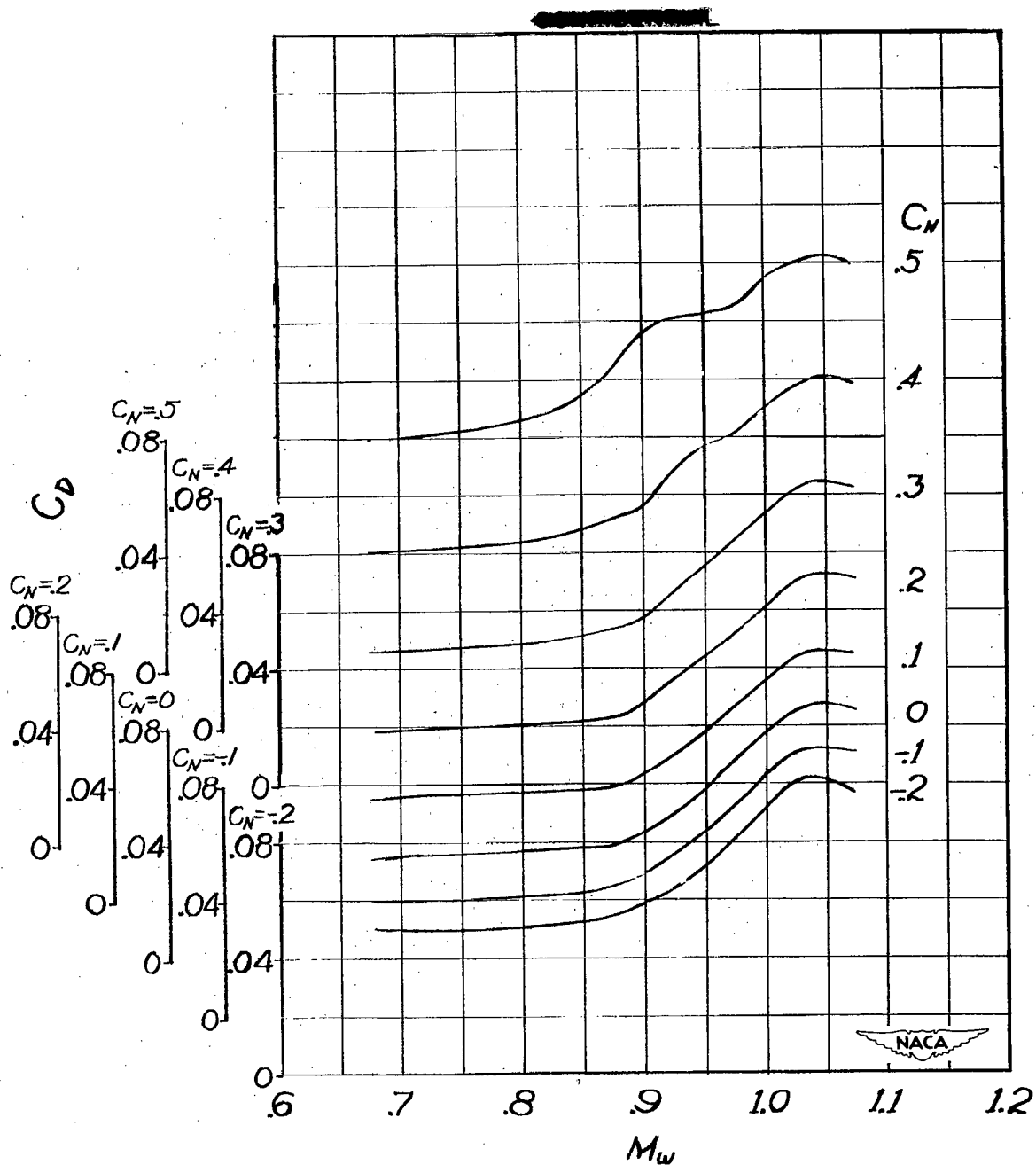
~~CONFIDENTIAL~~



(b) Complete model with unswept wing.

Figure 19.— Continued.

~~CONFIDENTIAL~~

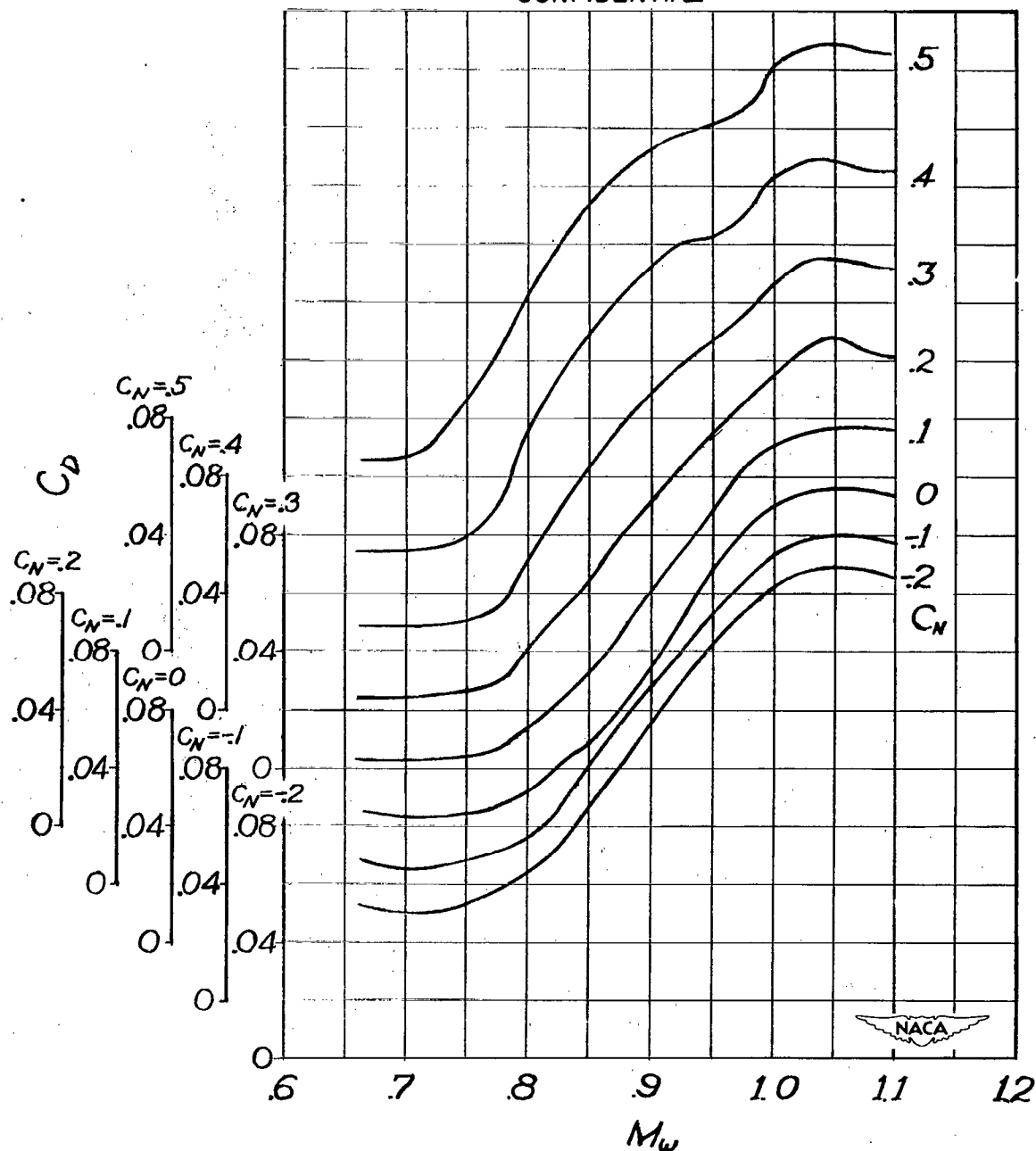


(c) Model less empennage with swept wing.

Figure 19.- Continued.

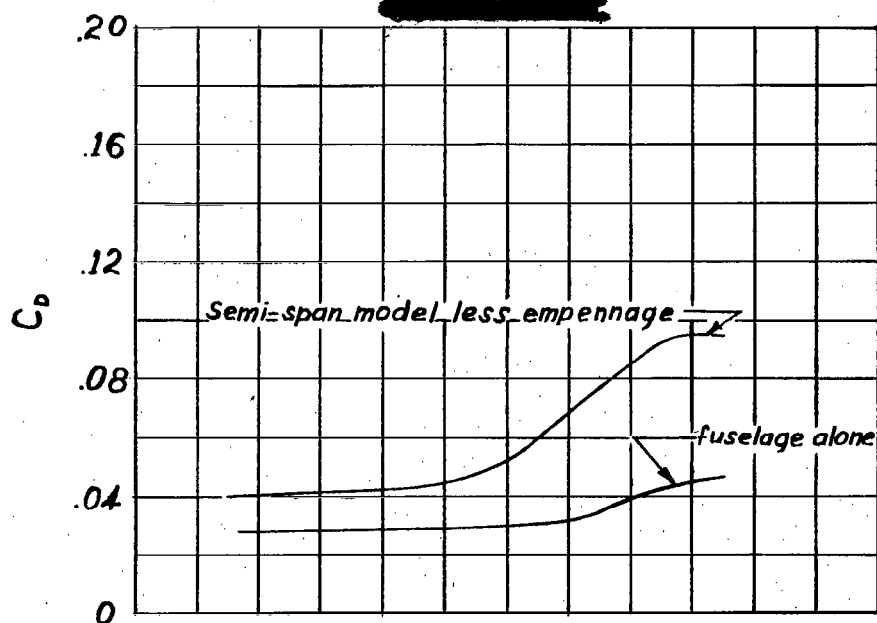
~~CONFIDENTIAL~~

CONFIDENTIAL

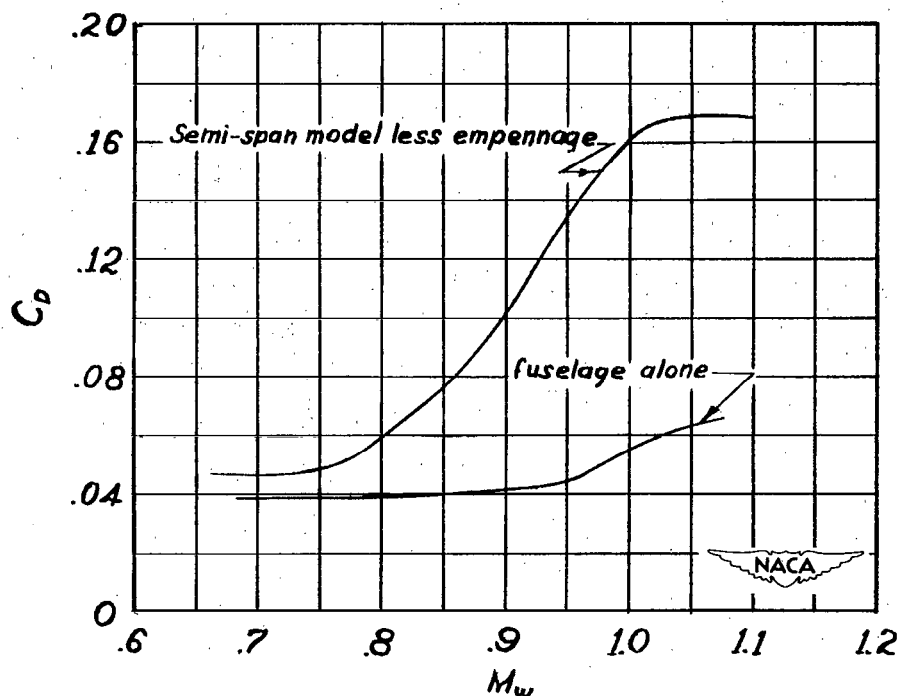


(d) Model less empennage with unswept wing.

Figure 19.— Concluded.



(a) With swept wing.  $\alpha = 0^\circ$



(b) With unswept wing.  $\alpha = 0^\circ$

Figure 20.— Variation with Mach number of drag coefficient for the semispan fuselage alone and for semispan model less empennage.

NASA Technical Library



3 1176 01437 9839